

*NCC 2-711*

*FINAL  
INFORMAL  
SET  
93116*

**LOW BANDWIDTH ROBUST CONTROLLERS FOR FLIGHT  
NASA Grant NCC 2-711**

June 1991 - December 1992

Final Report

by

Dr. Daniel J. Biezad  
Principal Investigator  
(805) 756-5126

and

Hwei-Lan Chou  
Graduate Student

Aeronautical Engineering Department  
California Polytechnic State University  
San Luis Obispo, CA 93407

presented to

Mr. Glenn Gilyard  
NASA Technical Officer  
(805) 258-3724

May 1993

Propulsion and Performance Branch, D-2112  
XRP PO 273, NASA Dryden  
Edwards, CA 93523

## Table of Contents

| <u>Item</u>   | <u>Page</u> |
|---|-------------|
| List of Figures   | iii         |
| List of Tables  | vi          |
| Preface   | vii         |
| Acknowledgements  | vii         |
| Synopsis  | viii        |
| Abstract  | ix          |
| <br>  |             |
| 1. Introduction   | 1           |
| <br>  |             |
| 2. Strategy of Throttle-Only Flight Control                 | 3           |
| 2.1 Pitch Control   |             |
| 2.2 Yaw-Roll Control  |             |
| 2.3 Speed Control   |             |
| 2.4 Couple Throttles Command to Stick/<br>Thumbwheel Motion |             |
| <br>  |             |
| 3. Boeing 720 Linear Model                                  | 4           |
| <br>  |             |
| 4. Engines and Bare Airframe System Survey                  | 4           |
| 4.1 Engines   |             |
| 4.2 Bare Airframe   |             |
| <br>  |             |
| 5. Overview of Quantitative Feedback Theory (QFT)           | 6           |
| <br>  |             |
| 6. Quantitative Feedback Theory (QFT) Control Design        | 8           |
| 6.1 System Modeling   |             |
| 6.2 Performance Specification                               |             |
| 6.3 Airplane Parameter Uncertainty                          |             |
| 6.4 Controller and Prefilter Design                         |             |
| <br>  |             |
| 7. Results and Discussion                                   | 14          |
| <br>  |             |
| 8. Conclusions and Recommendations                          | 17          |
| <br>  |             |
| References  | 18          |
| <br>  |             |
| Appendix A: B-720 Configurations                            |             |
| <br>  |             |
| Appendix B: Papers Produced in Support of this Grant        |             |

## List of Figures

- Figure 1. Boeing-720
- Figure 2. Boeing-720 simulation cockpit
- Figure 3. Comparison of the longitudinal open-loop response of the B-720 linear and nonlinear model, 20% step throttle cmd, nominal configuration
- Figure 4. Comparison of the lateral open-loop response of the B-720 linear and nonlinear model, 5% differential throttle, nominal configuration
- Figure 5. Comparison of the longitudinal open-loop response of the B-720 modified linear and nonlinear model, nominal configuration
- Figure 6. Engine spooling block diagrams and Engine  $\delta$  to  $\delta_{TC}$
- Figure 7. Pitch rate to thrust bode
- Figure 8. QFT unit feedback control structure
- Figure 9. Equivalent MISO systems of a 3x3 MIMO system
- Figure 10. Typical close loop tracking specification
- Figure 11. Typical disturbance rejection specification
- Figure 12. U contour construction
- Figure 13. Performance bounds, U contour, and the optimal  $L_o$
- Figure 14. A prefilter is needed to fulfill the performance specification
- Figure 15. Flight-path-angle control block diagram
- Figure 16. Bank-angle control block diagram
- Figure 17. Flight-path-angle control with inner q-loop closed
- Figure 18. Bank-angle control with inner  $\beta$ -loop closed
- Figure 19. Performance specification in time domain for approach and landing of B-720 TOFC

- Figure 20. Performance specification in frequency domain for approach and landing of B-720 TOFC
- Figure 21. Transfer function  $G_{\theta_m}^y$ , its performance bounds  $B(j\omega)$ , and U contour on Nichols Chart; flight-path-angle control
- Figure 22. Open-loop transfer function,  $L_{\theta_m}^y$ , on Nichols Chart
- Figure 23. Frequency plot of the close-loop transfer function  $T_{y_m}^y$  with no prefilter
- Figure 24. Frequency plot of the close-loop transfer function  $T_{y_m}^y$  with prefilter
- Figure 25. Transfer function  $G_{\beta_m}^\phi$ , its performance bounds  $B(j\omega)$ , and U contour on Nichols Chart; bank-angle control
- Figure 26. Open-loop transfer function,  $L_{\beta_m}^\phi$ , on Nichols Chart
- Figure 27. Frequency plot of the close-loop transfer function  $T_{\beta_m}^\phi$  with no prefilter
- Figure 28. Frequency plot of the close-loop transfer function  $T_{\beta_m}^\phi$  with prefilter
- Figure 29. B-720 augmented control, step flight-path-angle response with no turbulence, nominal configuration
- Figure 30. B-720 augmented control, step bank-angle response with no turbulence, nominal configuration
- Figure 31. B-720 augmented control, step flight-path-angle response with turbulence, nominal configuration
- Figure 32. B-720 augmented control, step bank-angle response with turbulence, nominal configuration
- Figure 33. Flight-path-angle and throttle response to full-forward stick deflection, nominal configuration
- Figure 34. Bank-angle and throttle response to full-right stick deflection - QFT compensation, nominal configuration
- Figure 35. Response to full-right stick deflection - Heuristic compensation, nominal configuration

Figure 36. Bank-angle response under turbulence due to c.g.  $\beta$

Figure 37. Bank-angle response under turbulence due to nose boom  $\beta$

Figure 38. Robustness of the flight-path-angle control

Figure 39. Robustness of the bank-angle control

## **List of Tables**

- Table 1. Investigation of Longitudinal Feedback Parameter**
- Table 2. Investigation of Lateral Feedback Parameter**
- Table 3. QFT Performance Specification**
- Table 4. Flight Configurations for B-720 Approach and Landing**
- Table 5. Longitudinal Mode Comparison**
- Table 6. Lateral Mode Comparison**

## **PREFACE**

The statements and conclusions of this report are those of the authors and not necessarily those of the California Polytechnic State University, San Luis Obispo. The evaluations described in this document are based solely on the results of tests conducted by the authors during this project.

This report does not constitute a standard, regulation or specification. The mention of commercial products, their source, or their use in connection with materials reported herein is not to be construed as either an actual or implied endorsement of such products.

## **ACKNOWLEDGEMENTS**

The authors gratefully acknowledge the sponsored research by NASA, and in particular acknowledge and thank Mr. Glenn Gilyard and Mr. Bill Burcham for their technical support, guidance, and encouragement throughout this project.

The material in this report was prepared and written by Professor Daniel Biezad and Graduate Student Hwei-Lan Chou; and edited by ARDFA Program Assistant Sue Dotson.

## SYNOPSIS

This final report for NASA Grant NCC 2-711 cover reporting period June 1992 through December 1992. The report analyzes the longitudinal and lateral flying qualities of Propulsive-Only Flight Control (POFC) for a Boeing 720 aircraft model. Using Quantitative Feedback Theory (QFT), performance results from compensators are documented and analyzed. This report is also the first draft of a graduate thesis to be presented by Hwei-Lan Chou. The final thesis document will be presented to NASA when completed later this year.

The latest landing metrics, related to bandwidth criteria and based on the Neal-Smith approach to flying qualities prediction, were used in developing the performance criteria for the controllers. The compensator designs were tested on the NASA simulator and exhibited adequate performance for piloted flight. There was no significant impact of QFT on the performance of POFC in either the longitudinal or lateral modes of flight. This was attributed to the physical limits of thrust available and the engine rate of response, both of which severely limited the available bandwidth of the closed-loop system.

## Abstract

Through throttle manipulations, engine thrust can be used for emergency flight control for multi-engine aircraft. Previous study by NASA Dryden has shown the use of throttles for emergency flight control to be very difficult. In general, manual fly-by-throttle is extremely difficult - with landing almost impossible, but control augmentation makes runway landings feasible. Flight path control using throttles-only to achieve safe emergency landing for a large jet transport airplane, Boeing 720, was investigated using Quantitative Feedback Theory (QFT). Results were compared to an augmented control developed in a previous simulation study. The control augmentation corrected the unsatisfactory open-loop characteristics by increasing system bandwidth and damping, but increasing the control bandwidth substantially proved very difficult. The augmented pitch control is robust under no or moderate turbulence. The augmented roll control is sensitive to configuration changes.

# 1. Introduction

Through throttle manipulations, engine thrust was found useful in providing some controllability for multi-engine aircraft in emergency situations with severe or complete flight control system failures (such as hydraulic system failures). Aircraft flight control systems are extremely reliable. Current generation aircraft utilize multiple and independent control surfaces, hydraulics, sensors, control computers, and control cables to achieve a high level of control system redundancy and reliability. Although rare, severe flight control system failures do occur.

NASA Dryden has studied the use of throttles for emergency flight control for a range of airplanes<sup>1-5</sup>. Many multi-engine airplanes exhibited some degree of useful control capability with the throttles. In general, flying an aircraft in manual mode using throttles-only requires a tremendous pilot workload and landing is considered extremely difficult to almost impossible. Control augmentation, using feedbacks and direct coupling of the throttle command to stick/thumbwheel motion, has greatly improved flying qualities, and ground simulation landings can be achieved.

The primary aim of this current study on Throttles-Only Flight Control (TOFC) is to develop an augmented flight path control using throttles-only to achieve safe emergency landings. Application of TOFC on a large four-engine jet transport airplane, Boeing 720 (B-720) (Figure 1), is investigated. An augmented B-720 TOFC, developed and implemented on a high fidelity B-720 flight simulator (Figure 2) by NASA Dryden<sup>2</sup>, had obtained good pilot rating by increasing the control bandwidth and the phugoid and Dutch-roll damping<sup>2</sup>.

This report presents an alternative control design technique based on Quantitative Feedback Theory (QFT) to further improve the Dutch-roll damping and to increase the control bandwidth for better handling qualities. The control design uses a linearized B-720 model derived from perturbations of the full non-linear equations of motion about trim at an approach and landing flight condition.

A robust controller is highly desirable for systems with plant parameter uncertainty (such as an aircraft undergoing configuration changes). The QFT technique<sup>6-9</sup> was chosen because it allowed designers to specify a desired close-loop response and a performance specification, and then built a controller to meet the specification. Most of all, the technique can incorporate plant parameter uncertainty and plant disturbances into the control system design by converting them into design constraints and then design a controller to have the system satisfy the imposed constraints. The controller thus designed guarantees robust performance over full range of the plant uncertainty while keeping the disturbance effect to the system minimum.

The desired performance specification may not always be achieved within the given control actuation and rate limits. However, the transparency of the QFT technique throughout the design process preserves many of the insights which are lost

in several of the modern control techniques and thus provides control designers with valuable information about the system under investigation. QFT also provides a quantitative relationship between the amount of uncertainty and feedback (i.e. the magnitude of feedback is determined in proportion to the amount of uncertainty, therefore, reduces the possibility of overdesign).

In this report, the strategy of flight control using throttles-only is introduced. The fidelity of the linear B-720 model is examined. An overview of QFT with step-by-step procedures is provided, and its application on the design of an augmented flight path control using throttles-only for approach and landing of B-720 is presented in a summary fashion. Control design results using QFT are compared to the augmented control developed in a previous simulation study.

## Nomenclature, Abbreviations, and Acronyms

|                     |  |
|---------------------|--|
| (a)                 | short form of (s+a)                                  |
| c.g.                | center of gravity                                    |
| $C_{l\beta}$        | non dimensional yaw-roll coupling derivative         |
| $C_{mu}$            | non dimensional velocity-pitch coupling derivative   |
| D.R.                | Dutch-roll   |
| $G_{in}^{out}$      | transfer functions                                   |
| $K_q$               | pitch rate feedback gain                             |
| $K_\gamma$          | flight path angle feedback gain                      |
| $K_\beta$           | sideslip angle feedback gain                         |
| $K_\phi$            | bank angle feedback gain                             |
| q                   | pitch rate (deg/sec)                                 |
| QFT                 | Quantitative Feedback Theory                         |
| s.p.                | short period   |
| TOFC                | Throttle-Only Flight Control                         |
| z                   | thrust (lbs)   |
| $\delta$            | engine rpm   |
| $\delta T_c$        | stick input (full deflection=1 unit)                 |
| $\gamma$            | flight path angle (deg)                              |
| $\theta$            | pitch angle (deg)                                    |
| $\beta$             | angle of sideslip (deg)                              |
| $\phi$              | bank angle (deg)                                     |
| $\omega_i$          | natural frequency                                    |
| $\zeta$             | damping ratio  |
| $[\zeta, \omega_n]$ | short form for $s^2 + 2\zeta\omega_n s + \omega_n^2$ |

## 2. Strategy of Throttles-Only Flight Control

The propulsion system of a multi-engine aircraft can be used for heading and flight path control. Differential throttles is applied to control roll through yaw, and symmetric throttles is applied to control pitch. Speed control by throttles becomes ineffective when control systems fail. Other means may be used to change the airplane speed as described in below. Throttles are coupled to stick/thumbwheel for easier and more conventional control handling.

### 2.1 Pitch Control

Symmetric throttles induces a phugoid mode and a speed change, which in turn generates a pitching moment change through speed stability effects- $C_{mu}$ . This is the primary source of pitch control. Pitch control may also be generated by other factors such as pitching moment change due to thrust line offset, flight path angle change due to the vertical component of thrust, and an instant pitching moment change generated by engines mounted at different vertical levels, as in the case of B-720.

### 2.2 Yaw-Roll Control

Differential thrust generates sideslip, which in turn generates rolling moment changes through wing dihedral and sweep effect- $C_{lp}$ . Roll is controlled by applying differential throttles to achieve the desired bank angle and thus to make turns and heading changes.

### 2.3 Speed Control

Retrimming speed by the use of throttles becomes ineffective when primary control surfaces are locked due to control systems failure. When control system failure occurs at speeds other than landing speed, retrimming to an acceptable landing speed may be accomplished by using other techniques such as lowering flaps (assuming the electrically controlled flaps are operative), extending landing gears, moving cg. aft, varying stabilizer deflection, or varying the speed between the low and high mounted engines.

### 2.4 Couple Throttle Command to Stick/Thumbwheel Motion

Direct coupling of the throttle command to stick/thumbwheel motion has eased the pilot's handling of control. The airplane can be controlled in a conventional fashion, such as pitch up with stick forward or pitch down with stick aft.

### 3. B-720 Linear Model

The B-720 linear model is derived from perturbations of the full nonlinear equation of motion about trim and is completely decoupled in longitudinal and lateral dynamics. All control states and inputs are perturbed independently at the steady state of a desired trim condition. The inputs are thrust from each engine. There are four configurations given for the study of approach and landing of B-720 TOFC. The state-space representation of the linear model of these configurations are listed in Appendix A. Of the four configurations shown, configuration 1 is the nominal configuration for baseline design.

The fidelity of the linear model was examined by comparing the open-loop response of the linear model with the nonlinear model as shown in Figures 3 and 4. The longitudinal response of the linear model was about 30% less in magnitude than the nonlinear model, and was, therefore, modified by a correction factor of 1.3 (Figure 3). The longitudinal linear model after modification closely portrays the longitudinal nonlinear model (Figure 5). Linear design analysis utilized a computer control package "Program CC" to assist the design<sup>10</sup>.

The lateral response depicted in Figure 4 shows that the linear model would closely follow the nonlinear model as long as the small perturbation assumption is not violated, i.e. the command input should be of a small magnitude and a short duration. Figures 3 and 4 also illustrate that for the nonlinear model, a flight path angle command would induce little coupling in roll/yaw, while a bank angle command would induce pronounced pitch coupling. Coupling between longitudinal and lateral modes is completely absent for the linear model.

### 4. Engines and Bare Airframe System Analysis

#### 4.1 Engines

Spool-up and spool-down engine dynamics for the B-720 engine are shown in Figure 6a<sup>12</sup>. The empirical transfer function developed is given in short form notation by

$$G_{\delta_{TC}(\omega)}^{z(lbs)} = \frac{275}{(.55)(5)}$$

This equation is illustrated in Figure 6b over low frequency ranges up to 1.0 rad/sec.

## 4.2 Bare Airframe

It is apparent from the engine Bode diagram in Figure 6b illustrates that severe bandwidth attenuation would occur beyond frequencies of 1 rad/sec. Therefore, it may not be possible to increase the closed-loop bandwidth beyond 1 rad/sec within the range of available thrust. This can be seen in the pitch rate "q" to thrust "z" transfer function,  $G_{\delta_{TC}(\omega)}^{q(\text{deg/sec})}$  (refer to Appendix A), of the bare airframe shown in Figure 7. The full-order transfer function  $G_{\delta_{TC}(\omega)}^{q(\text{deg/sec})}$  shows that 80 dB of gain must be added to yield a crossover frequency beyond 1 rad/sec. This corresponds to 10,000 lbs of full thrust from each engine, which is not practical for approach and landing.

A low order fit to  $G_{\delta_{TC}(\omega)}^{q(\text{deg/sec})}$  is also depicted in Figure 7 and is very accurate near the phugoid frequency. Piloted flight of the unaugmented aircraft was consistently a level 3<sup>2</sup>. The main difficulties were the lightly damped phugoid and the low bandwidth throttle control.

The accuracy of the low order fit near the phugoid frequency means that, to a first order approximation<sup>12</sup>, the phugoid frequency and damping are found from the following equation:

$$2\zeta\omega_n = -X_u + \frac{M_u(X_\alpha - g)}{M_\alpha}$$

$$\omega_n^2 = \frac{-g(Z_u - \frac{M_u}{M_\alpha}Z_\alpha)}{U_0}$$

Conventional transport aircraft can be shown to be roughly proportional to  $M_u$ .

It should be strongly noted here for the classic case of  $M_u=0$  and for negative values of  $M_u$  (Mach tuck) that the aircraft cannot be practically flown with throttle alone unless rotational control in pitch is added and difficulties will also be encountered as  $M_\alpha$  becomes small (aft c.g. location). Both of these cases require the addition of an effective rotational controller about the pitch axis. This may be achieved by using differential inboard and outboard thrust, provided the inboard engines are a different distance from the aircraft xy-plane than the outboard engines. These configuration characteristics determine the innate capability for throttles-only piloted control.

## 5. Overview of Quantitative Feedback Theory

QFT is a frequency domain control technique that uses a fairly straightforward and transparent design approach<sup>69</sup>. To apply QFT, systems are usually modeled in a unit feedback form (Figure 8) where all blocks may present scalar (SISO) or matrix (MIMO) system transfer functions. For MIMO systems, a  $m \times m$  MIMO system can be converted into a  $m^2$  - equivalent multi-input single-output (MISO) loops (Figure 9). QFT techniques allow designers to specify a desired performance specification with performance tolerance and then incorporate the tolerance with the plant uncertainty and system disturbances to form the design constraints: the performance bounds and the U contour (Figures 10, 11 and 12).

The design constraints are then placed on a Nichols Chart together with the nominal plant transfer function,  $P_o$ . A controller will be selected to reshape  $P_o$  to form  $L_o$  (the nominal open-loop transfer function) as to have  $L_o$  satisfying all the design constraints of performance bounds and U contour (Figure 13). By having  $L_o$  satisfy all the design constraints, if possible within the given control actuation and rate limits, the system is guaranteed robust over the full range of plant uncertainty. However, the system may not completely meet the performance specification (Figure 14). A prefilter is usually required to further reshape the system to fully meet the specification. The prefilter design is implemented on a Bode plot.

The basic design procedures of the QFT technique for minimum phase systems are accomplished by the following four steps:

- 1) Model the system in a unit feedback form to apply QFT. A  $m \times m$  MIMO system can be converted into a  $m^2$ -equivalent MISO system and the coupling between loops can be considered disturbance input (Figures 8 and 9).
- 2) Specify the desired close-loop frequency response performance specification. Figure 10 shows the construction of a desired close-loop performance specification with an upper bound,  $B_u$ ; a lower bound,  $B_L$ ; a tolerance,  $\delta_R$ ; and a maximum peak magnitude,  $M_m$ .

The tolerance,  $\delta_R$ , is specified to obtain robust performance, and the maximum  $M_m$  is specified to obtain a desired system damping. The upper bound is generally synthesized by an underdamped second order close-loop transfer function (T.F.),  $T_u(s)$  and the lower bound by an overdamped close-loop T.F.,  $T_L(s)$  with figures of merit such as settling time, rise time, peak overshoot or damping ratio, and natural frequency, etc.

A desired disturbance performance specification (Figure 11) needs only an upper bound to confine the disturbances. The objective of the technique is to design a controller such that the variation of the response due to plant uncertainty lies within the specified boundaries and the effect of disturbance is minimized, that is to have:

$$B_L(\omega) \leq |T_R(j\omega)| \leq B_U(\omega)$$

$$|T_D(j\omega)| \leq |M_D(j\omega)|$$

$$|T_{Dz}(j\omega)| \leq |M_D(j\omega)|$$

3) Convert the performance tolerance,  $\delta_R$ , and the maximum  $M_m$ , onto Nichols Chart to form the design constraints: the performance bounds,  $B_o(j\omega_i)$ , and the U contour.

i) Performance bounds are curves on the Nichols Chart that are determined by matching the magnitude of the range of plant uncertainty with the magnitude of the performance tolerance,  $\delta_R$ . Therefore, satisfying this constraint guarantees the variation of the system response due to plant uncertainties will be no greater than  $\delta_R$ . There is a performance bound for each frequency.

ii) On the Nichols Chart, the U contour is a M-circle that has the magnitude of  $M_m$ , with part of the circle stretched for uncertainty at high frequencies (same as the length V shown in Figure 12). By having the open-loop response not penetrating the U contour, the system's damping will be guaranteed no less than the damping correlating to  $M_m$ . The construction of a U contour is shown in Figure 12.

4) Reshape the nominal plant transfer function,  $P_o$ . Gain/pole/zero compensation may be placed on  $P_o$  to reshape it to satisfy the design constraints. After reshaping,  $P_o$  becomes  $L_o$ , and the compensation chosen forms the controller,  $G_c$ , as can be depicted from the relationship:

$$L_o = P_o * G_c$$

To satisfy the design constraints,  $L_o$  should not penetrate the U contour, while each frequency  $\omega_i$  on  $L_o$  should be kept on and above its corresponding  $B_o(j\omega_i)$ . The U contour, the performance bounds and the optimal  $L_o$  of an example problem are shown in Figure 13.

5) After reshaping, the system is guaranteed robust over the full range of plant uncertainty, i.e.  $\delta_T(j\omega_i) \leq \delta_R(j\omega_i)$  (Figure 14). However, the system may not have met the performance specifications completely. A prefilter is usually required to further reshape the system to fully meet the specification.

## 6. Quantitative Feedback Theory Control Design

A QFT computer control package was used to assist the QFT design<sup>8</sup>. The program is to be used for minimum-phase plants only, i.e., the plants should have no zeros in the right half s-plane, therefore, only the gain curve of the desired performance will be specified and satisfied. For nonminimum-phase plant, the phase of the desired close-loop performance shall also be specified and satisfied.

### 6.1 System Modeling

The block diagrams of flight-path-angle control and bank-angle control are presented in Figures 15 and 16. The inner pitch-rate ( $q$ ) loop and sideslip-angle ( $\beta$ ) loop were first closed with  $G_{\delta_q}^{\delta_q} = 1$ ,  $K_q = 60$  and  $G_{\delta_\beta}^{\delta_\beta} = 10$ ,  $K_\beta = 4$ , respectively, which were the heuristic settings chosen by investigating the properties of the inner loop. Tables 1 and 2 summarize the investigation:

Table 1. Investigation of Longitudinal Feedback Parameter

| Feedback Parameter | Phugoid                         | Mode       |
|--------------------|---------------------------------|------------|
|                    | $\zeta$                         | $\omega_n$ |
| $q$                | Increase<br>(Require high gain) | No change  |
| $\gamma$           | No change                       | Increase   |

Table 2. Investigation of Lateral Feedback Parameter

| Feedback Parameter | Lateral Phugoid |                | Dutch          | Roll       |
|--------------------|-----------------|----------------|----------------|------------|
|                    | $\zeta$         | $\omega_n$     | $\zeta$        | $\omega_n$ |
| $p$                | Increase        | Increase       | Decrease       | No change  |
| $r$                | Small increase  | No change      | Small increase | No change  |
| $\beta$            | Small decrease  | Small increase | Increase       | No change  |
| $\varphi$          | Increase        | Increase       | Small increase | No change  |

To apply QFT, with the inner loop closed, the outer loops are rearranged in a unit feedback form as shown in Figures 17 and 18.

## 6.2 Performance Specification

To obtain good handling qualities, the close-loop response for each of the  $\gamma$ - and  $\phi$ - loops, which are also the pilot control open-loops, should have the following characteristics:

- 1) A bandwidth,  $\omega_{\omega B} \approx 2$  rad/sec for landing of a transport aircraft<sup>11</sup>.
- 2) A k/s gain curve slope (-20 dB/decade) around the crossover frequency,  $\omega_c$ <sup>12</sup>.

A desired close-loop specification was synthesized based upon these two requirements, and is shown in Figure 19, which has a k/s slope near  $\omega_c \approx 1.5$  rad/sec (with  $\omega_{\omega B} \approx 2$  rad/sec) and a corner frequency,  $\omega_{\text{corner}} \approx 0.8$  rad/sec.

The desired close-loop specification is synthesized in the following four steps:

- 1) Synthesize the initial  $B_U$  and  $B_L$ .  $B_U$  is usually modeled by an underdamped simple second order close-loop T.F.,

$$T_u(s) = \frac{\omega_n^2}{s^2 + 2\zeta\omega_n s + \omega_n^2},$$

while  $B_L$  modeled by an overdamped simple second order close-loop T.F.,

$$T_l(s) = \frac{k}{(s + \sigma_1)(s + \sigma_2)}, \text{ where } \sigma_1 \text{ and } \sigma_2 \leq \omega_n.$$

With a desired performance specification of  $\zeta = .6$  and  $\omega_n = .8$  rad/sec, this yields:

$$T_u(s) = \frac{.64(s+1)}{s^2 + .96s + .64} \text{ and } T_l(s) = \frac{.385}{(s+.55)(s+.7)}$$

- 2) Add a pole to  $T_l(s)$  to widen the  $\delta_n$  at high frequencies. This yields:

$$T_l(s) = \frac{.77}{(s+.55)(s+.7)(s+2)}$$

This is required by the Bode derived theorem which states that  $\int_0^\infty L_m S_p^T d\omega = 0$ ,

i.e. the reduction in sensitivity  $S_p^T$  at the lower frequencies must be compensated by an increase in sensitivity at the higher frequencies.

- 3) Add a zero at 1 rad/sec to increase the gain slope from -40 dB/decade to -20 dB/decade. This yields:

$$T_u(s) = \frac{.64(s+1)}{s^2 + .96s + .64} \quad \text{and} \quad T_L(s) = \frac{.77(s+1)}{(s+.55)(s+.7)(s+2)}$$

- 4) Raise the whole synthesized gain curve until a  $\omega_{\text{WB}} \approx 2$  rad/sec is obtained.

The magnitude of  $B_u$ ,  $B_L$  and  $\delta_n$  at each frequency can thus be obtained and are shown in Table 3.

Table 3. QFT performance specification

| Frequency(rad/sec) | 0.1  | 0.3  | 0.5  | 0.7  | 1.0  | 2.0  | 5.0   |
|--------------------|------|------|------|------|------|------|-------|
| $B_u$ (dB)         | 17.0 | 17.0 | 17.3 | 16.0 | 13.0 | 2.0  | -13.0 |
| $B_L$ (dB)         | 16.8 | 15.0 | 12.3 | 9.9  | 4.6  | -7.1 | -23.0 |
| $\delta_n$ (dB)    | 0.2  | 2    | 5    | 6.1  | 8.4  | 9.1  | 15.0  |

### 6.3 Airplane Parameter Uncertainty

Four configurations are provided for the study of approach and landing of B-720 throttles-only flight control. The flight condition of these configurations are summarized in Table 4. Configuration 1 is the nominal configuration for baseline design.

Table 4. Flight Configurations for B-720 Approach and Landing

| Config. Number | Weight (lbs) | Altitude (Ft MSL) | Airspeed (Knots) | Flaps (%) | Gear up/down |
|----------------|--------------|-------------------|------------------|-----------|--------------|
| 1              | 140,000      | 4,000             | 160              | 0         | up           |
| 2              | 140,000      | 4,000             | 145              | 30        | up           |
| 3              | 160,000      | 4,000             | 175              | 0         | up           |
| 4              | 140,000      | 4,000             | 155              | 30        | up           |

A plant transfer function with parameter uncertainty is usually described in a maximum and minimum format in order to form the plant uncertainty template, which will then be used to determine the performance bounds constraint. An example of a plant with parameter uncertainty described in a maximum and minimum format is shown below:

Example

For a plant transfer function

$$G(s) = \frac{ka}{(s+a)}, \text{ where the parameter variations are: } 1 < k < 10 \text{ and } 1 < a < 10$$

then,

$$G(s) \text{ min.} = \frac{1}{s+1} \quad \text{and} \quad G(s) \text{ max.} = \frac{100}{s+100}$$

For  $\gamma$ - and  $\phi$ - feedback loops, the minimum and maximum values of the transfer functions  $G_{\theta_{in}}^{\gamma}$  and  $G_{\beta_{in}}^{\phi}$ , determined from the four given configurations, are shown below:

For  $\gamma$ -feedback loop:

The  $G_{\theta_{in}}^{\gamma(\text{deg})}$  of the nominal configuration (config. 1) is:

$$G_{\theta_{in}}^{\gamma(\text{deg})} \text{ config. 1} = \frac{.01(.203)[.37, 3.01]}{(.562)[.624, .111][.441, 1.57]} \quad (5.25)$$

and the min. and max.  $G_{\theta_{in}}^{\gamma(\text{deg})}$  are:

$$G_{\theta_{in}}^{\gamma(\text{deg})} \text{ min.} = \frac{.0053 (.162) [.35, 3.01]}{(.40) [.42, 1.48] [.66, .01]} \quad (5.19)$$

$$G_{\theta_{in}}^{\gamma(\text{deg})} \text{ max.} = \frac{.01 (.28) [.46, 3.43]}{(.58) [.45, 1.57] [.92, .14]} \quad (5.24)$$

**For  $\varphi$ - feedback loop:**

The  $\mathbf{G}_{\beta_{in}(\text{deg})}^{\phi(\text{deg})}$  of the nominal configuration(config. 1) is:

$$\mathbf{G}_{\beta_{in}(\text{deg})}^{\phi(\text{deg})} \text{ nominal} = \frac{.09 [.47, 3.65]}{(.98) [.81, .15] [.26, 1.07]} (5.02)$$

and the min. and max. of  $\mathbf{G}_{\beta_{in}(\text{deg})}^{\phi(\text{deg})}$  are:

$$\mathbf{G}_{\beta_{in}(\text{deg})}^{\phi(\text{deg})} \text{ min.} = \frac{.06 [.45, 3.65]}{(.98) [.60, .15] [.24, .93]} (5.01)$$

$$\mathbf{G}_{\beta_{in}(\text{deg})}^{\phi(\text{deg})} \text{ max.} = \frac{.09 [.61, 4.33]}{(1.03) [1.0, .20] [.29, 1.09]} (5.02)$$

The QFT control package, used to assist the design, allows the designer to input plant parameter variations by entering the transfer function's maximum and minimum values for gain, first order poles and zeros, and second order poles and zeros. The program forms the plant uncertainty template with the given maximum and minimum values, then uses its CAD capability to graphically determine the performance bounds required for the design. There are tradeoffs between plant parameter uncertainty and system performances. The wider the spread of the parameter uncertainty, the more restricted the constraints; consequently more compensation is required. Therefore, the performance specification may need to be relaxed when there is not enough control power to provide all the compensation that is required.

**6.4 Controller and Prefilter Design**

Pole/zero/gain compensation may be required to reshape the plant transfer functions of the  $\gamma$ - and  $\varphi$ - feedback loops,  $\mathbf{G}_{\theta_{in}}^{\gamma}$  and  $\mathbf{G}_{\beta_{in}}^{\phi}$ , and to satisfy performance bounds and U contour constraints. On a Nichols Chart, adding a gain will raise the transfer function curve, while a zero will bend the curve to the right, and a pole will bend the curve to the left. The compensation chosen forms the controller,  $\mathbf{G}_c$ . After reshaping  $\mathbf{G}_{\theta_{in}}^{\gamma}$  and  $\mathbf{G}_{\beta_{in}}^{\phi}$  become, respectively,  $\mathbf{L}_{\theta_{in}}^{\gamma}$  and  $\mathbf{L}_{\beta_{in}}^{\phi}$  (the open-loop transfer functions of the  $\gamma$ - and  $\varphi$ -loops), where  $\mathbf{L}_{\theta_{in}}^{\gamma} = \mathbf{G}_{\theta_{in}}^{\beta_{in}} * \mathbf{G}_{\theta_{in}}^{\gamma}$  and  $\mathbf{L}_{\beta_{in}}^{\phi} = \mathbf{G}_{\beta_{in}}^{\beta_{in}} * \mathbf{G}_{\beta_{in}}^{\phi}$ . Each frequency  $\omega_i$  on  $\mathbf{L}_{\theta_{in}}^{\gamma}$  and  $\mathbf{L}_{\beta_{in}}^{\phi}$  should be placed on and above its corresponding performance bounds,  $B_o(j\omega_i)$ , to assure robust performance. In addition,  $\mathbf{L}_{\theta_{in}}^{\gamma}$  and  $\mathbf{L}_{\beta_{in}}^{\phi}$  must not penetrate the U contour in order to obtain the desired damping.

**Longitudinal Flight-Path-Angle Control:** Transfer function  $\mathbf{G}_{\theta_{in}}^{\gamma}$  and its performance bounds,  $B_o(j\omega_i)$ , and U contour are displayed on a Nichols Chart in Figure 21. All frequency points on  $\mathbf{G}_{\theta_{in}}^{\gamma}$  are below their corresponding  $B_o(j\omega_i)$ , hence reshaping is

required (Figure 21). A pure gain compensator,  $G_c = G_{\gamma}^{\theta_{in}} = 16$ , raises the curve to just touching the U contour (Figure 22). Several lead compensators were tried to further reshape the  $G_{\theta_{in}}^{\gamma}$  to satisfy all  $B_o(j\omega_i)$  while not penetrating the U contour. The lead compensators tried had increased the bandwidth and robustness; however, they also reduces the output  $\gamma$  to a very small value(e.g., an output  $\gamma=2$  degree for a full stick input). Therefore, only the pure gain of 16 is chosen as the compensator, this left the  $B_o(j\omega_i)$  unsatisfied. The frequency response of the close-loop transfer function,  $T_{\gamma_{in}}^{\gamma}$  (where  $T_{\gamma_{in}}^{\gamma} = L_{\sigma_{\gamma}}^{\gamma} / (1 + L_{\sigma_{\gamma}}^{\gamma}) = (G_{\sigma_{\gamma}}^{\theta_{in}} * G_{\theta_{in}}^{\gamma}) / (1 + G_{\sigma_{\gamma}}^{\theta_{in}} * G_{\theta_{in}}^{\gamma})$ ), is shown in Figure 23. It can be seen in Figure 23 that  $\delta_{\tau}$ (the spread between  $T_{max}$  and  $T_{min}$ ) had exceeded the  $\delta_R$  over the frequency range 0.1 to 0.7 rad /sec as a result of  $L_{\sigma_{\gamma}}^{\gamma}$  not satisfying the performance bounds over that frequency range. To have any frequency,  $\omega_i$ , on  $L_{\sigma_{\gamma}}^{\gamma}$  higher than its corresponding  $B_o(j\omega_i)$  will result in  $\delta_{\tau}(j\omega_i) \geq \delta_R(j\omega_i)$ , while lower than  $B_o(j\omega_i)$  will result in  $\delta_{\tau}(j\omega_i) \geq \delta_R(j\omega_i)$ . As can be depicted in figure 23, further modification is required to fully meet the prescribed specification. A prefilter of a pure gain of 6.5 proved most effective in increasing the bandwidth and met the prescribed specification. The frequency response after the prefilter is applied is shown in Figure 24.

**Lateral Bank-Angle Control:** Transfer function  $G_{\beta_{in}}^{\phi}$  and its performance bounds,  $B_o(j\omega_i)$ , and U contour are displayed on a Nichols Chart in Figure 25. Notice that  $G_{\beta_{in}}^{\phi}$  is not only below all performance bounds  $B_o(j\omega_i)$  but it also penetrates the U contour. Therefore, more than just a pure gain is required to reshape  $G_{\beta_{in}}^{\phi}$ . A controller,  $G_{\sigma_{\phi}}^{\beta_{in}} = (s+.15)/(s+1.5)$ , was added to  $G_{\beta_{in}}^{\phi}$  to reshape it and prevent it from penetrating the U contour, but it was not successful in satisfying all of the  $B_o(j\omega_i)$ . After reshaping,  $L_{\sigma_{\phi}}^{\beta_{in}}$  is shown on a Nichols Chart in Figure 26. The frequency plot of the close-loop transfer function,  $T_{\beta_{in}}^{\phi}$ , where  $T_{\beta_{in}}^{\phi} = L_{\sigma_{\phi}}^{\beta_{in}} / (1 + L_{\sigma_{\phi}}^{\beta_{in}}) = (G_{\sigma_{\phi}}^{\beta_{in}} * G_{\beta_{in}}^{\phi}) / (G_{\sigma_{\phi}}^{\beta_{in}} * G_{\beta_{in}}^{\phi})$ , with no prefilter applied yet is shown in Figure 27. A lead compensator of  $(S+1)/(S+2)$  is added to haunch up the severely deteriorated curve at frequency over 1 rad /sec and to increase the phase margin. A lag compensator of  $(S+0.25)/(S+0.15)$  is added to steepen the gain curve at low frequencies and to provide a smoother k/s curve for good pilot handling qualities. The close-loop response after adding the prefilter is shown in Figure 28 and the prefilter selected is  $15(S+0.25)(S+1)/((S+0.15)(S+2))$ .

## 7. Results and Discussion

The objective of this study is to improve the handling qualities for the approach and landing of B-720 TOFC by increasing the control bandwidth and the light Dutch-roll damping. The control bandwidth of TOFC depends primarily on the engine response to throttle command, and on the propulsion-induced low-frequency speed and dihedral stability effects, which are configuration-dependent, thus are fixed and unalterable. Therefore, the control engineer's only tools are compensation and feedback.

To improve control bandwidth is very difficult as can be depicted from the pitch rate to thrust bode in Figure 7. Full thrust of 10,000 lbs from each engine is required to yield a crossover frequency just beyond 1 rad/sec. This clearly shows how control bandwidth is limited by the control power (the engine) available.

For flight-path-angle control, pitch rate feedback was effective in increasing phugoid damping while  $\gamma$  feedback was effective in improving frequency of the phugoid mode. For bank-angle control,  $\beta$  feedback was found most effective in increasing Dutch-roll damping while  $\phi$  feedback is crucial to lateral phugoid damping. Yaw rate feedback, which is effective in damping Dutch-roll when rudder power is available, helps Dutch-roll damping and the lateral phugoid damping very little. Tables 5 and 6 compare the dynamic modes of the bare airframe with the dynamic modes of previous simulation designs, of QFT design and of heuristic design (heuristic compensation will be discussed later on page 19.) Transfer functions of  $\gamma$  to stick and  $\phi$  to stick for all the four configurations are listed in Appendix A.

Table 5. Longitudinal Mode Comparison

|                              | Density  | Phugoid   | Short Period | Engine    | Pre-filter | $G_{\gamma}^{\phi_{in}}$ | $G_{\phi}^{\phi_{in}}$ | $K_{\gamma}$ | $K_{\phi}$ |
|------------------------------|----------|-----------|--------------|-----------|------------|--------------------------|------------------------|--------------|------------|
| Bare Airframe                | (1.4E-6) | (.04,,13) | (.65,1.4)    | (.55)(5)  | -          | -                        | -                      | -            | -          |
| Simulation Augmented Control | (4.7E-6) | (.52,,24) | (.52,1.5)    | (.4)(5.2) | 10         | 1                        | 10                     | 1            | 4          |
| QFT Augmented Control        | (3.4E-6) | (.62,,32) | (.46,1.6)    | (.3)(5.2) | 6.5        | 16                       | 1                      | 1            | 60         |

GMAI  
1.18.10  
L.1077

Table 6. Lateral Mode Comparison

|                              |           | Dutch Roll | Roll  | Engine   | Pre-filter                     | $G_{e,\beta}^{in}$    | $G_{e,\beta}^{\delta_{TC}}$ | $K_{\phi}$ | $K_p$ | $K_{\beta}$ | $K_r$ |
|------------------------------|-----------|------------|-------|----------|--------------------------------|-----------------------|-----------------------------|------------|-------|-------------|-------|
| Bare Airframe                | (1.1E-4)  | (.12,.99)  | (1)   | (.55)(5) | -                              | -                     | -                           | -          | -     | -           | -     |
| Simulation Augmented Control | (.73,.35) | (.15,.99)  | (1)   | (5)      | 40                             | 1                     | 1                           | .5         | .5    | 1           | -     |
| QFT Augmented Control        | (.39)     | (.29,1.0)  | (1.5) | (.45)(5) | $\frac{2.5(.25)(1)}{(.15)(2)}$ | $\frac{(.15)}{(.15)}$ | 1                           | 1          | -     | 4           | -     |
| Heuristic Augmented Control  | (.75,.28) | (.22,1.0)  | (.9)  | (5)      | 40                             | 1                     | 1                           | .15        | .5    | 3           | 1     |

*PHI 1.5  
From  
in QFT*

For longitudinal control, pure gain compensation was used. Since the short period mode has a frequency around 1.5 rad/sec (which was beyond the frequency that throttles can control) the primary concern was to increase phugoid damping and frequency. The phugoid damping and frequency increased from 0.52 to 0.62 and from 0.24 rad/sec to 0.32 rad/sec, respectively. This increase of response frequency can also be depicted from the flight path angle response shown in Figure 29.

For lateral control, pole/zero compensation was used. The Dutch-roll damping was almost doubled, from 0.15 to 0.29. The simulation augmented control has a lateral phugoid mode [0.73, 0.35] which combines the spiral and the slow engine mode. This was replaced using the QFT design with two real root modes, (0.39) and (0.45), both with higher frequencies, therefore faster responses. The comparison of the responses is shown in Figure 30.

All plots in Figures 21 through 32 were obtained from nonlinear simulation runs at approach and landing conditions with major control surfaces (ailerons, elevator and rudders) locked while the electrical and mechanical systems, and the landing gear remained operative. Figure 33 through 35 shows the throttle response, and flight-path-angle and bank-angle tracking response to full stick deflection.

**Turbulence Response:** The response of the flight-path-angle control under intermediate turbulence is presented in Figure 31. Because of gust randomness, more than one simulation run was made to examine the tracking integrity under turbulence.

The bank angle tracking by QFT design does not perform well under intermediate turbulence (Figure 32). This could be caused by the larger  $K_{\beta}$  gain ( $K_{\beta}=4$ ) being used in the  $\beta$ -feedback loop by QFT design, while a  $K_{\beta}=1$  is used for the

simulation designed control. This larger  $K_\beta$  multiplies the gust-induced-sideslip four times before it was fed back to the airplane. This had a dramatic effect on the bank angle output due to 0.2 degree of sideslip angle would generate approximately 10 degrees of bank angle, owing to the large  $C_{l\beta}$  of B-720. The sideslip angle ( $\beta$ ) feedback is the only parameter that can effectively increase Dutch-roll damping for B-720 TOFC. A compromise seems necessary between lateral bank angle tracking and Dutch-roll damping.

Good Dutch-roll damping is associated with disturbance excitation of the lateral phugoid mode and results in poor tracking of bank angle. Lowering the feedback gain reduces Dutch-roll damping but also decreases the sensitivity of bank angle to disturbances, and thus makes the lateral phugoid mode less troublesome to the pilot when flying in turbulence.

During the investigation, it was found that the  $\beta$  being fed back into the B-720 simulator was the  $\beta$  at the c.g. instead of the  $\beta$  at the nose boom. The nose boom  $\beta$  is actually measured and fed back into a real airplane. The nose boom  $\beta$  was then modeled into the B-720 simulator and the results of the bank angle tracking under turbulence were fairly good. Figure 36 shows the bank-angle tracking under turbulence due to c.g.  $\beta$ , while Figure 37 shows two runs of bank-angle tracking under turbulence due to nose boom  $\beta$ . The  $\beta$  at the nose boom has two more terms caused by lateral and longitudinal offsets from the c.g. The dominant term is a function of roll rate. When this extra term was active in the feedback loop, lateral performance improved. However, there was some question concerning the correctness of the sign of the yaw rate term as implemented in the simulation. The effectiveness of yaw rate feedback for TOFC need to be further investigated.

A augmented control scheme heuristically determined that feedback  $p, r, \beta$  and  $\phi$  is investigated. The compensation of this control scheme is shown in Table 6. The yaw rate feedback is included in the control to improve bankangle tracking, the roll rate and bank angle feedbacks are included to increase the damping and frequency of the lateral phugoid mode while the  $\beta$  feedback to increase the Dutch-roll damping. The heuristic augmented control has a slightly slower response speed ( $\omega_n=0.28 < \omega_n=0.35$  of simulation augmented control), but a higher Dutch-roll damping ( $\zeta=.22 > \zeta=.147$  of simulation augmented control) which has successfully damped the Dutch-roll oscillation as can be seen in Figure 35.

The system response to configuration variations for  $\gamma$ -control and for  $\phi$ -control are shown in Figures 38 and 39, respectively. The robustness of the flight-path-angle control is improved by QFT as shown in Figure 38. The Dutch-roll oscillation in the original simulation compensation is taken out by QFT compensation; however, the tracking was not improved (Figure 39). Among the three augmented control developed, the heuristically determined augmented control presented the best robust performance

(with fairly good bank-angle tracking and no Dutch-roll oscillation.) Due to time constraints, the heuristic augmented control was not tested on the real-time nonlinear B-720 simulator.

## 8. Conclusions and Recommendations

Studies by NASA Dryden has shown that throttles can be used for emergency flight control. Manual fly-by-throttle is extremely difficult with landing almost impossible, but with control augmentation, runway landing is feasible.

Flight path control design using throttles-only to achieve safe emergency landing for a transport airplane, Boeing 720, was investigated. Augmented throttles-only flight path control built in a previous simulation study has made successful simulation landings. However, it showed light Dutch-roll damping and low control bandwidth. To increase the control bandwidth substantially proved very difficult. Differential throttles to engines mounted at different vertical levels to generate an instant pitching moment may be an effective way to increase the control bandwidth.

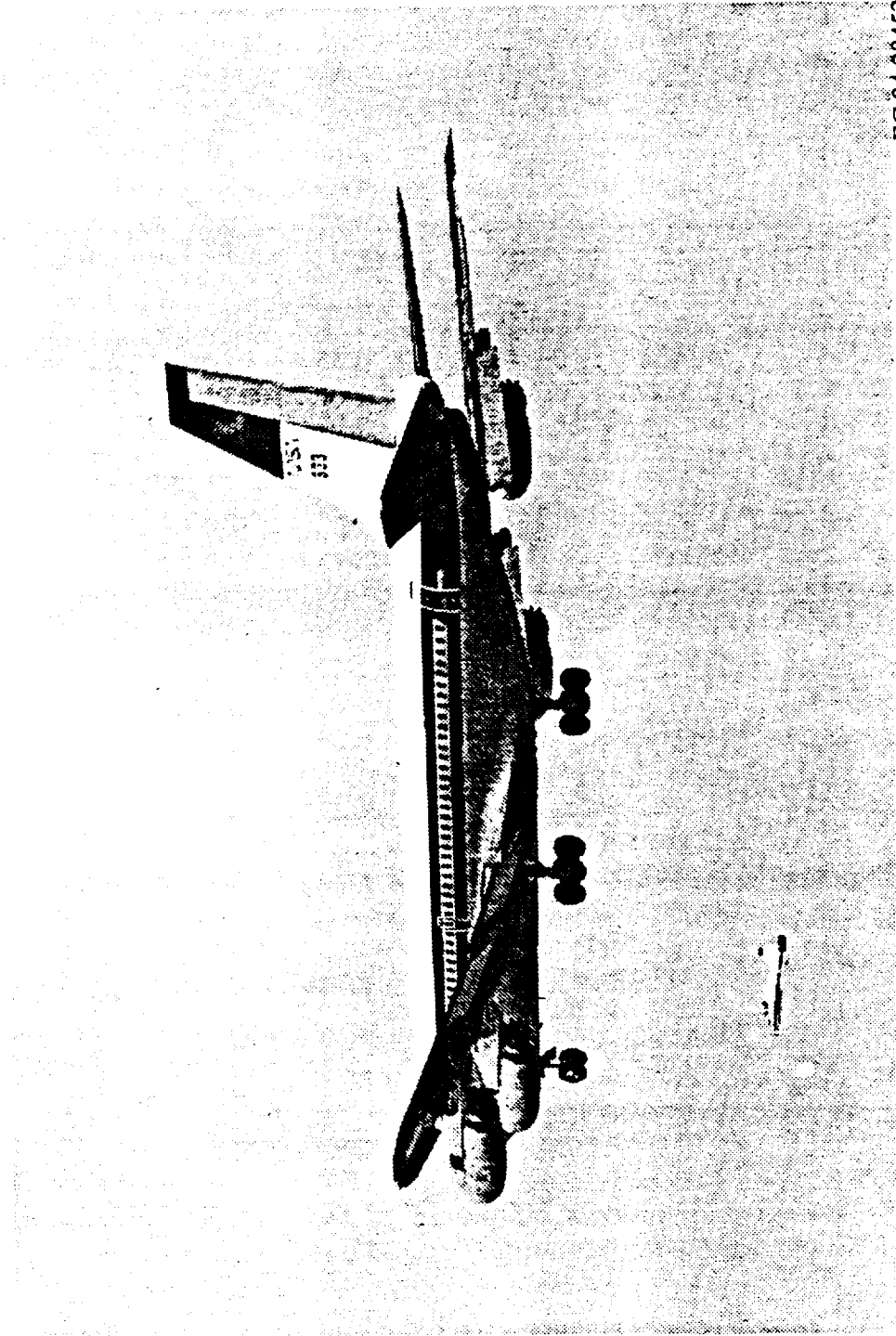
For throttles-only pitch control using QFT, the control bandwidth, tracking and control robustness were improved by QFT. For bank angle control, QFT has improved the Dutch-roll oscillation. However, the lateral phugoid becomes sensitive to configuration changes. A compromise is required between Dutch-roll and lateral phugoid damping given limited control power. Further investigation of the effects of yaw rate feedback is recommended.

## References

1. Burcham, F., Fullerton, G., Gilyard, G., Wolf, T., and J. Stewart. "A Preliminary Investigation of the Use of Throttles for Emergency Flight Control." NASA Dryden Document. 1991.
2. Gilyard, G., Conley, J., Le, J., and W. Burcham. "A Simulation Evaluation of a Four-Engine Jet Transport Using Engine Thrust Modulation for Flight Path Control." 27th Joint Propulsion Conference. June 24-26, 1991. Sacramento, CA.
3. Azzano, C.P. "A Preliminary Look at Optimal Multi-Variable Design of Propulsion-Only Flight Controllers for Jet Transport Aircraft." NASA Dryden Technical Report. Sept 21, 1990.
4. Biezad, D.J. "The Propulsive-Only Flight Control Problem," NAECON , Vol. 2. Dayton, Ohio. May 20-24, 1991. 494-500.
5. Biezad, D.J. and C.P. Azzano. "Designing Low Bandwidth Propulsive-Only Flight Controllers." AIAA Guidance, Navigation, and Control Conference Paper No. 91-2628CP. August 12-14, 1991. New Orleans, LA. 267-275.
6. Horowitz, I.M. and M. Sidi. "Synthesis of Feedback Systems with Large Plant Ignorance for Prescribed Time-domain Tolerances." Int. J. Control, Vol. 16. 1972. 287-309.
7. D'Azzo, J.J. and C.H. Houpis. "Linear Control System Analysis and Design Conventional and Modern." McGraw-Hill. 1988.
8. Yaniv, O. "Multiple-Input Single-Output (MISO) User Manual." Tel-Aviv University. 1991.
9. Horowitz, I.M. "Quantitative Feedback Design Theory (QFT)." Vol. 1. QFT Publication. 1992.
10. Thompson, Peter M. "Program CC Version 4 Reference Manual: Volume 1." Systems Technology, Inc. November 1988.
11. Biezad, D.J. and Hwei-Lan Chou. "Pilot-in-the-Loop Analysis of Propulsive-Only Flight Control Systems." NAECON. Dayton, Ohio. May 1992.
12. McRuer, D., Ashkenas, I., and D. Graham. "Aircraft Dynamics and Automatic Control." Princeton University Press. 1973.

13. Sarrafian, S.K. and B.G. Powers. "Application of Frequency Domain Handling Qualities Criteria to the Longitudinal Landing Task." NASA Technical Memorandum. August 1985.
14. MIL-STD-1797A. "Flying Qualities of Piloted Vehicles." Limited Distribution. ASD/ENES. Wright-Patterson AFB, Ohio. January 1990.
15. Gaffney, T. "Pilot in Sioux City Jet Crash Tells Story in Dayton." Dayton Daily News. March 26, 1991. Page 3-A.
16. Leavitt, P. "Crash Settlement." USA Today. March 27, 1991. Page 3-A.
17. Roskam, J. "Airplane Flight Dynamics and Automatic Flight Controls." Roskam Aviation and Engineering Corporation. Ottawa, Kansas. 1979.
18. Blakelock, J. "Automatic Control of Aircraft and Missiles." John Wiley and Sons, Inc. 1965.

## FIGURES



EC 84 28452

Figure 1. Boeing-720

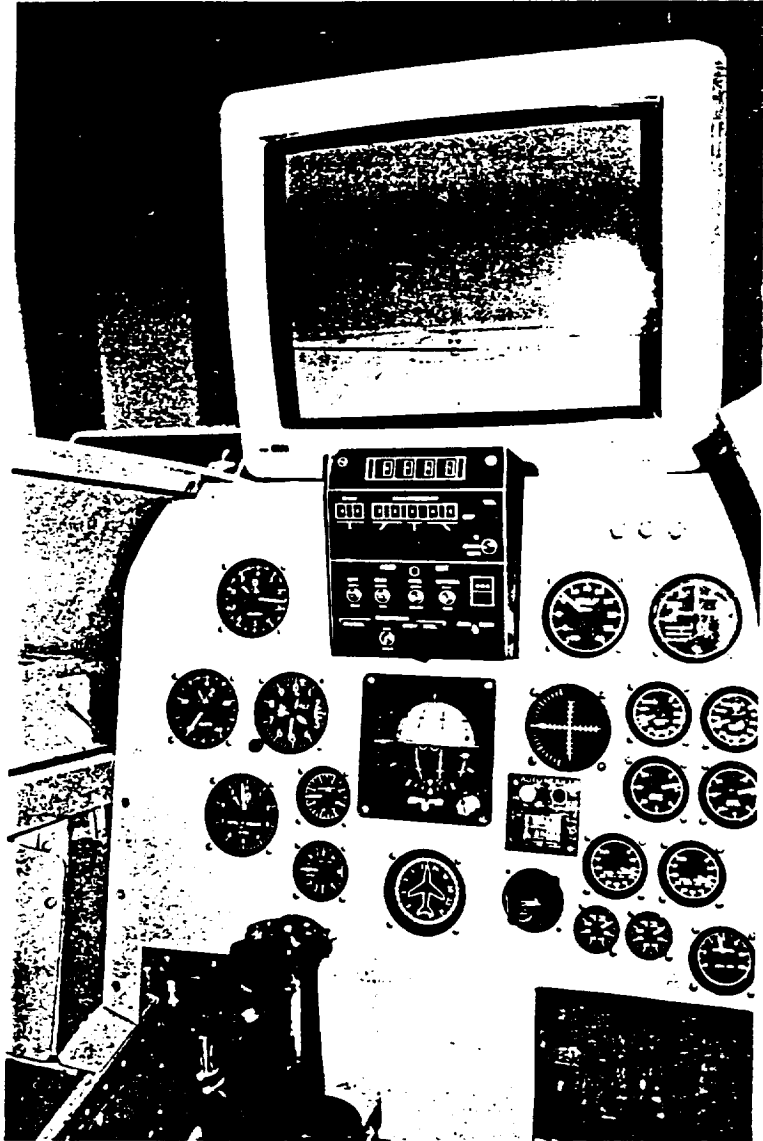


Figure 2. Boeing-720 simulation cockpit

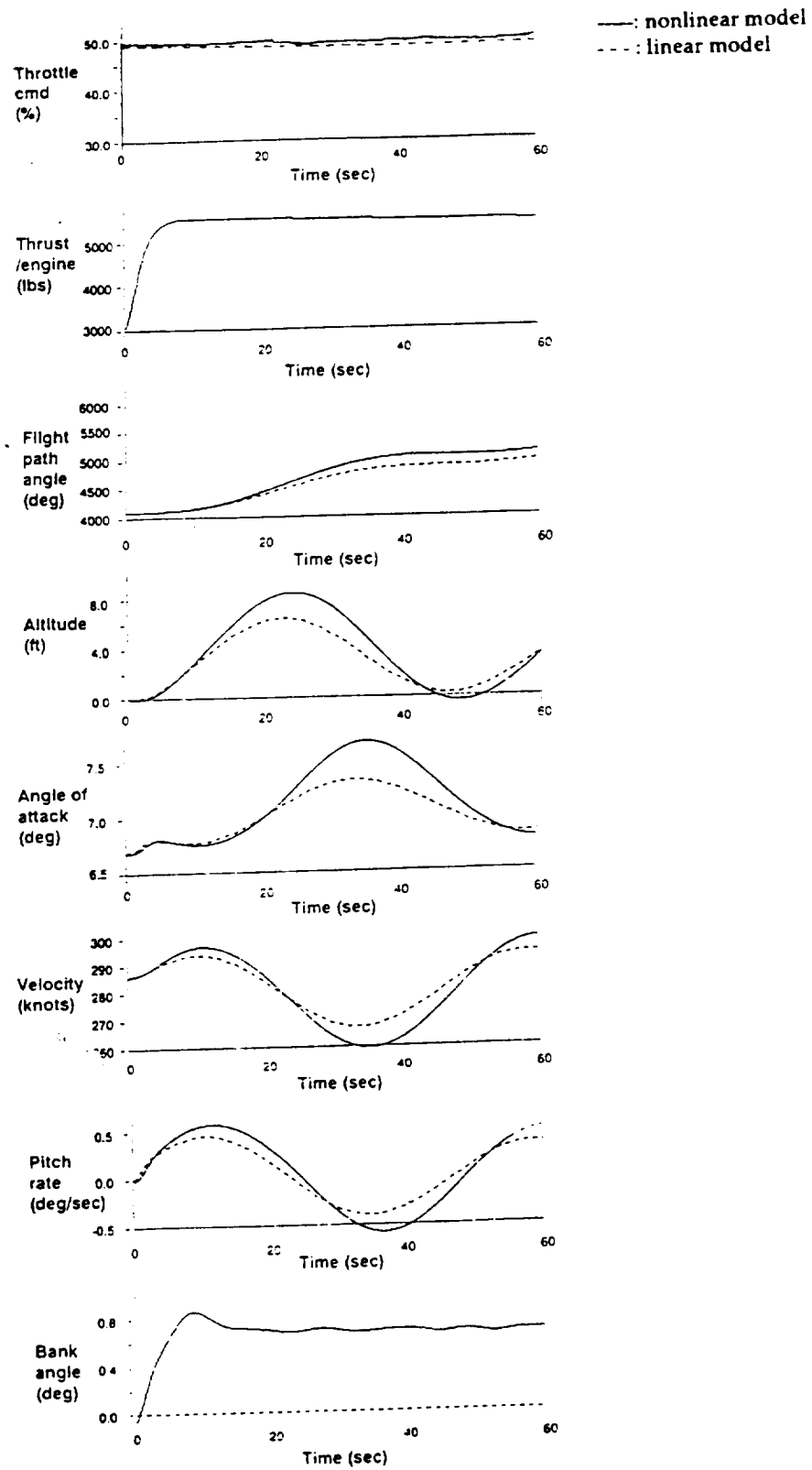


Figure 3. Comparison of the longitudinal open-loop response of the B-720 linear and nonlinear model, 20% step throttle cmd, nominal configuration

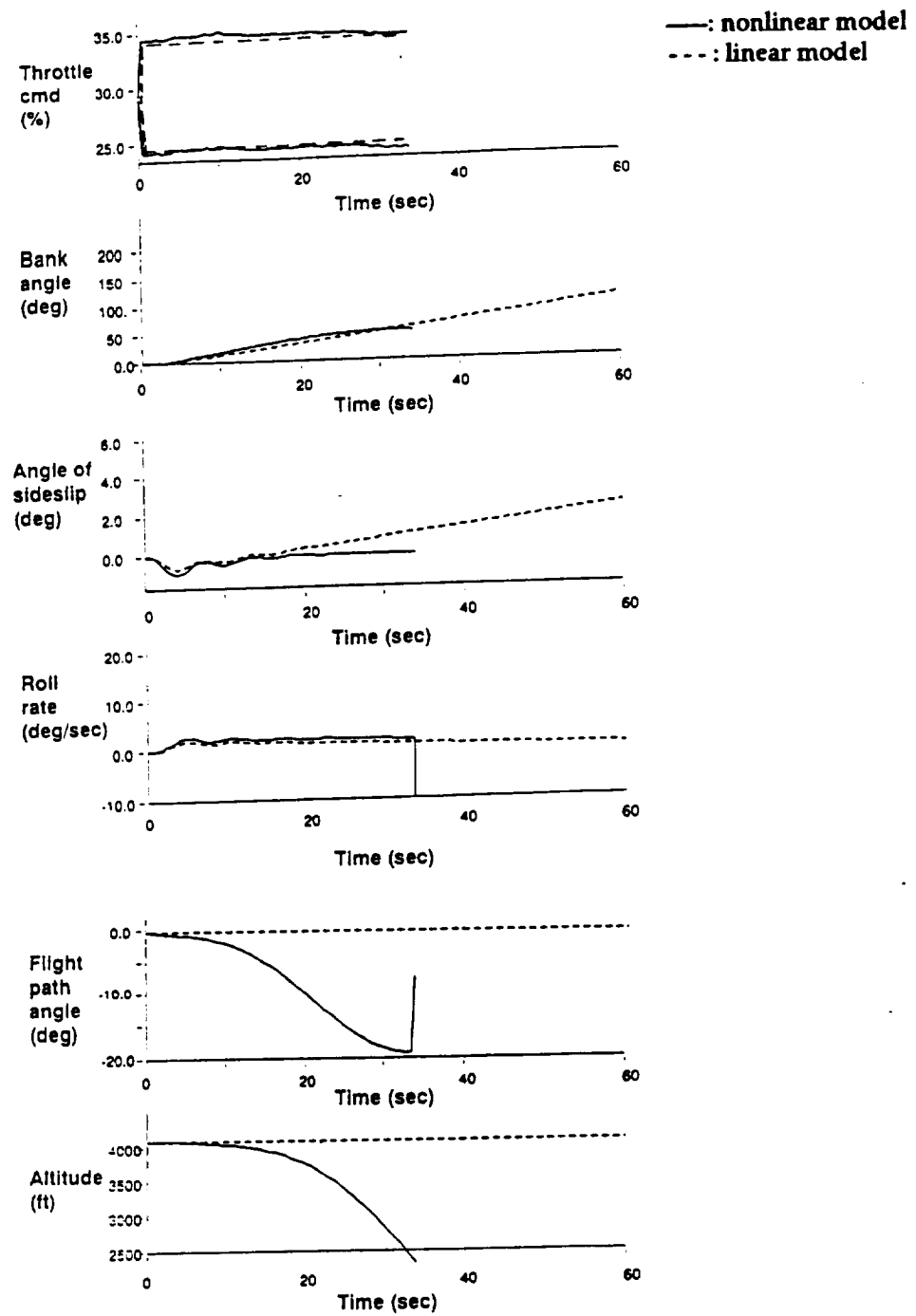


Figure 4. Comparison of the lateral open-loop response of the B-720 linear model and nonlinear model, 5% differential throttle, nominal configuration

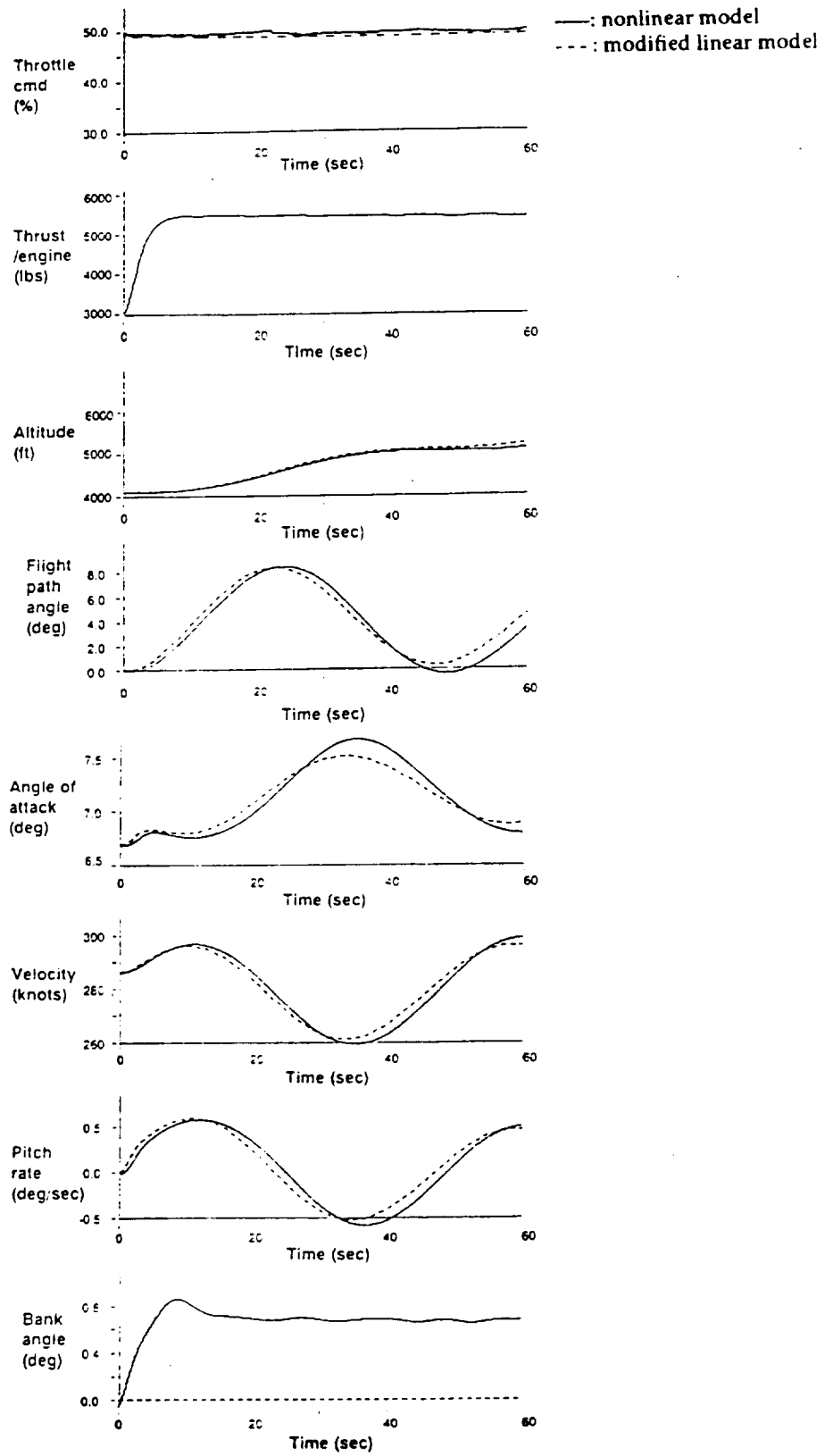
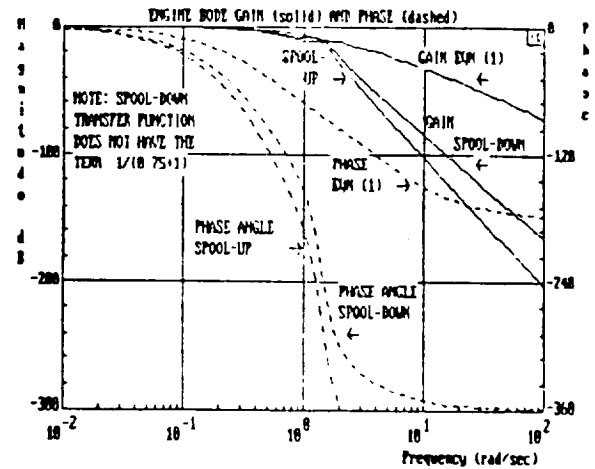
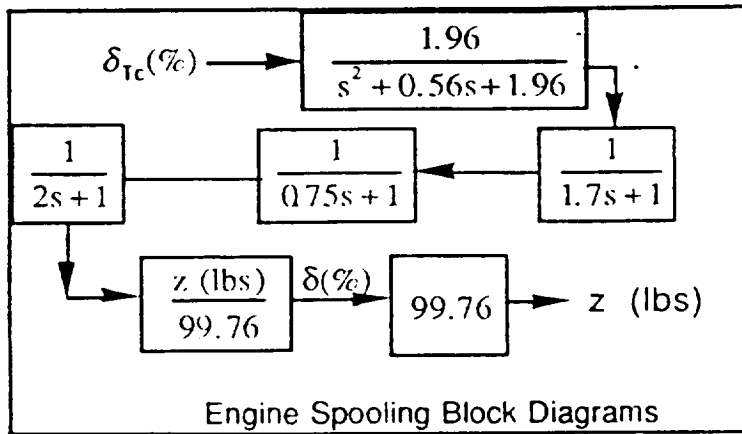


Figure 5. Comparison of the longitudinal open-loop response of the modified B-720 linear and nonlinear model, nominal configuration



Engine  $\delta$  to  $\delta_{Tc}$

Figure 6. Engine spooling block diagrams and Engine  $\delta$  to  $\delta_{Tc}$

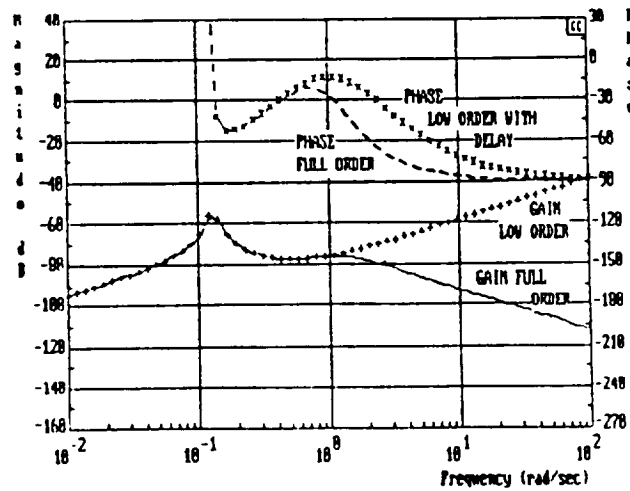
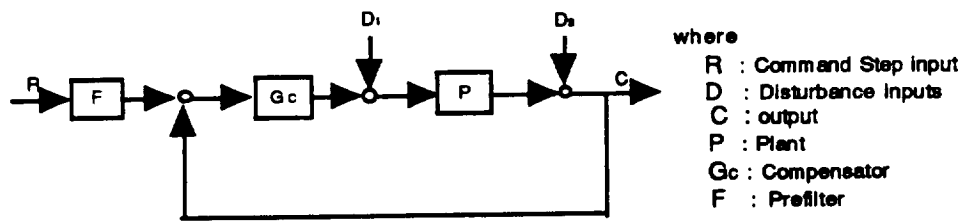


Figure 7. Pitch rate to thrust bode



The open loop transmission function, L, is defined as:

$$L = G_c * P \quad \text{and} \quad L_m L = L_m G_c + L_m P$$

The close loop transfer functions are:

$$\text{Tracking: } T_R = \frac{FL}{1+L} \quad \text{and} \quad L_m T_R = L_m F + L_m \frac{L}{1+L}$$

(D1=D2=0)

$$\text{Disturbance: } T_{D1} = \frac{P}{1+L}$$

(R=D2=0)

$$\text{Disturbance: } T_{D2} = \frac{1}{1+L}$$

(R=D1=0)

Figure 8. QFT unit feedback control structure

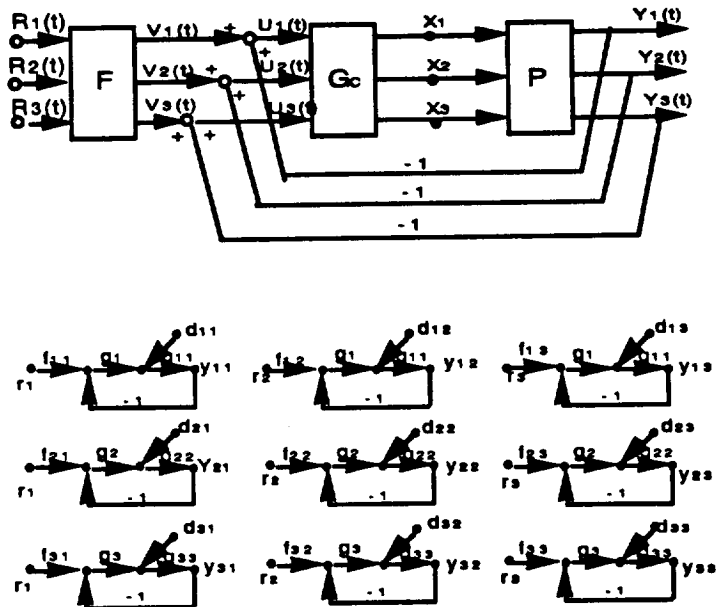


Figure 9. Equivalent MISO systems of a 3x3 MIMO system

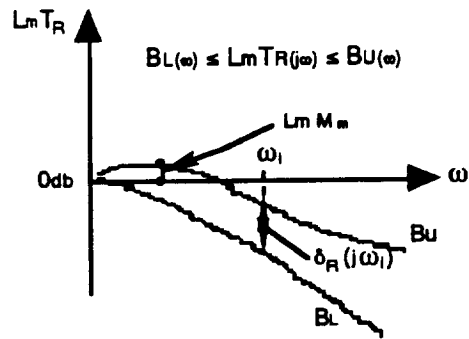


Figure 10. Typical close loop tracking specification

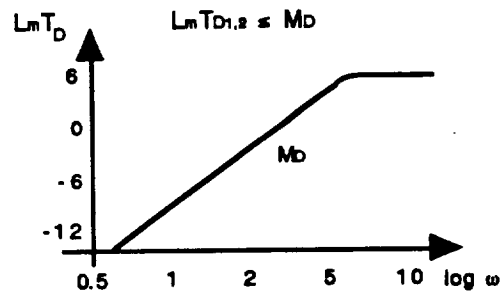


Figure 11. Typical disturbance rejection specification

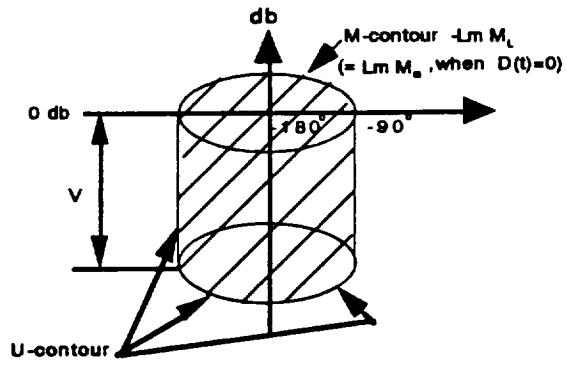


Figure 12. U contour construction

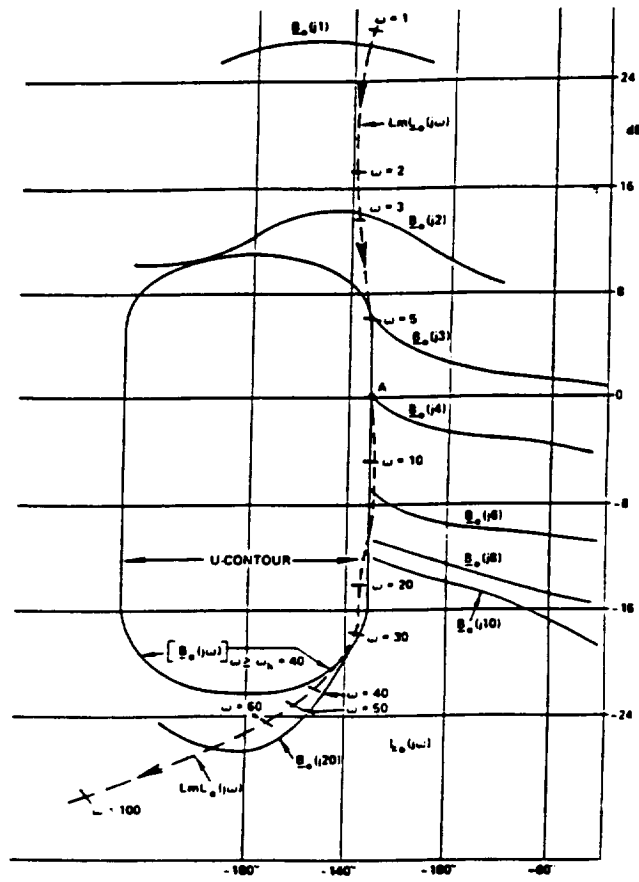


Figure 13. Performance bounds, U contour, and optimal  $L_0$

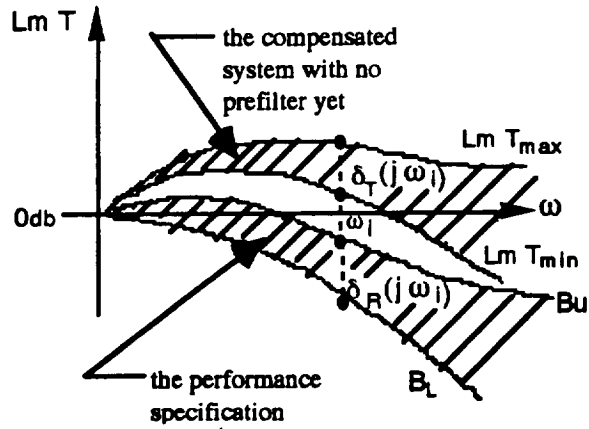


Figure 14. A prefilter is required to fulfill the performance specification

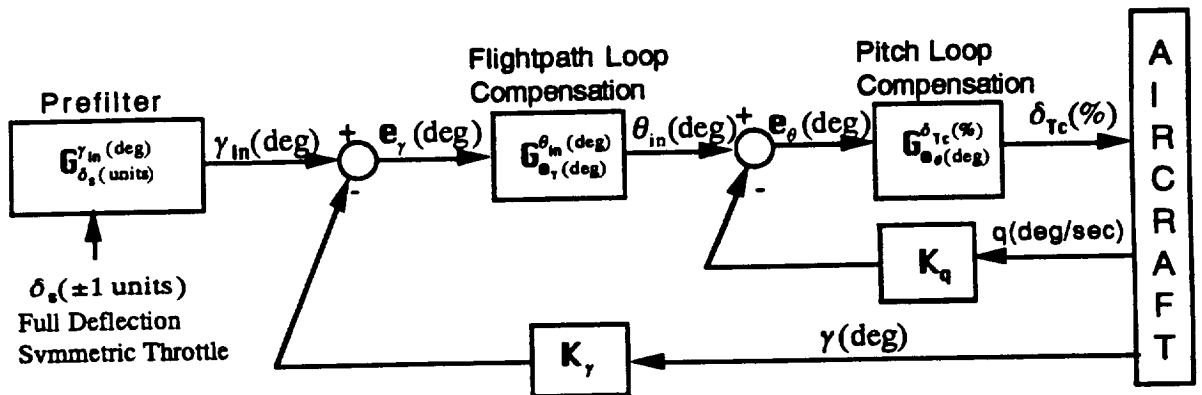


Figure 15. Flight-path-angle control block diagram

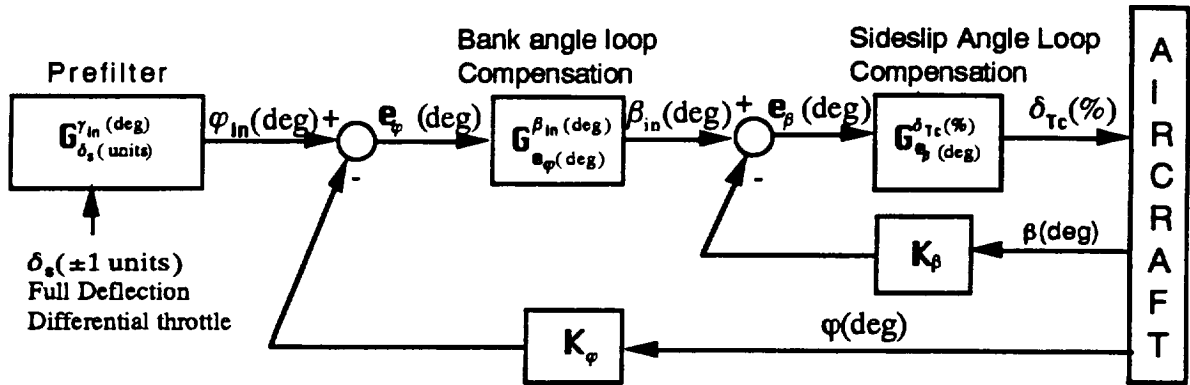


Figure 16. Bank-angle control block diagram

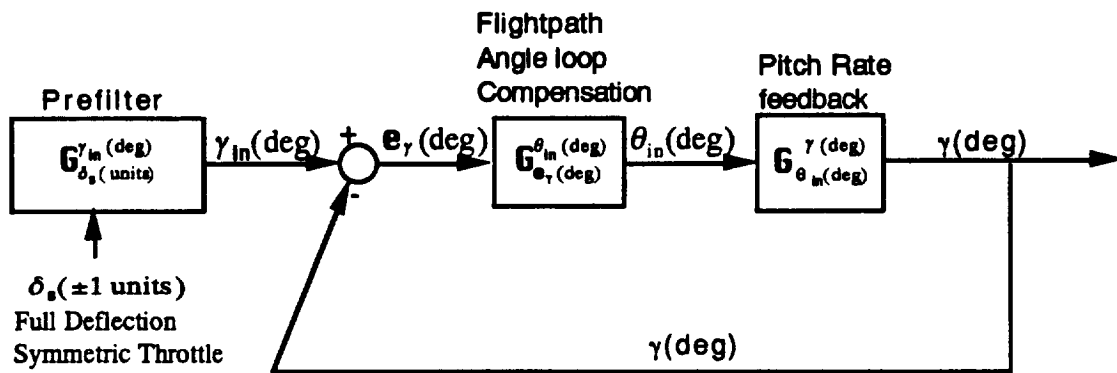


Figure 17. Flight-path-angle control with inner q-loop closed

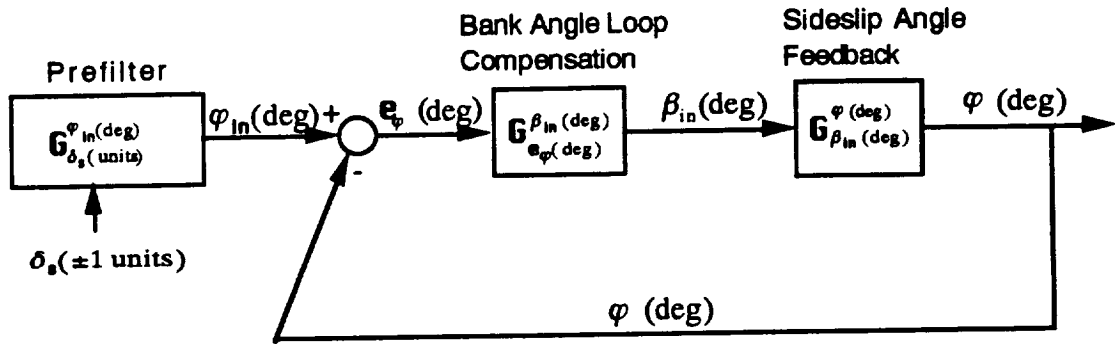


Figure 18. Bank-angle control with inner  $\beta$ -loop closed

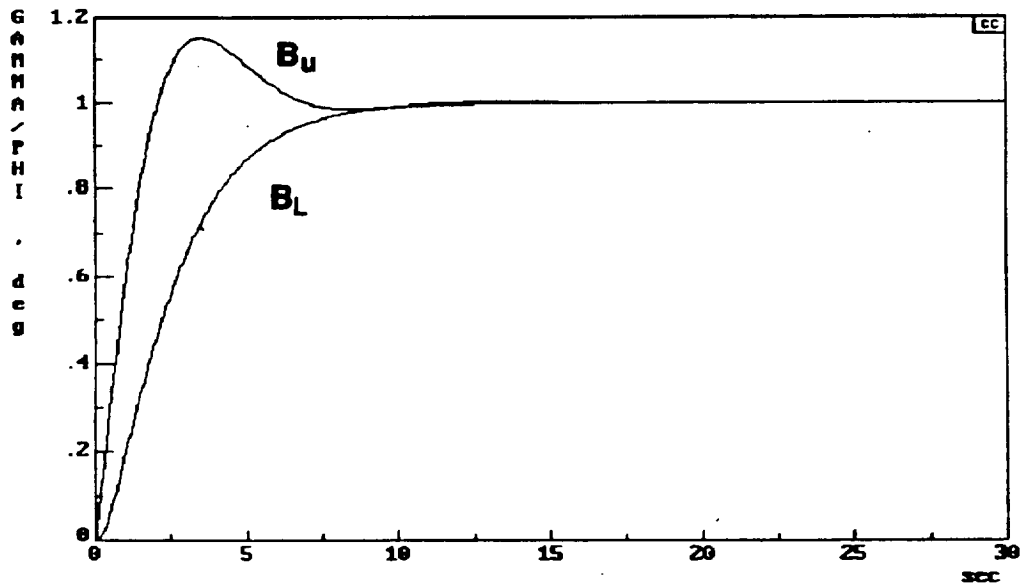


Figure 19. Performance specification in time domain for approach and landing of B-720 TOFC

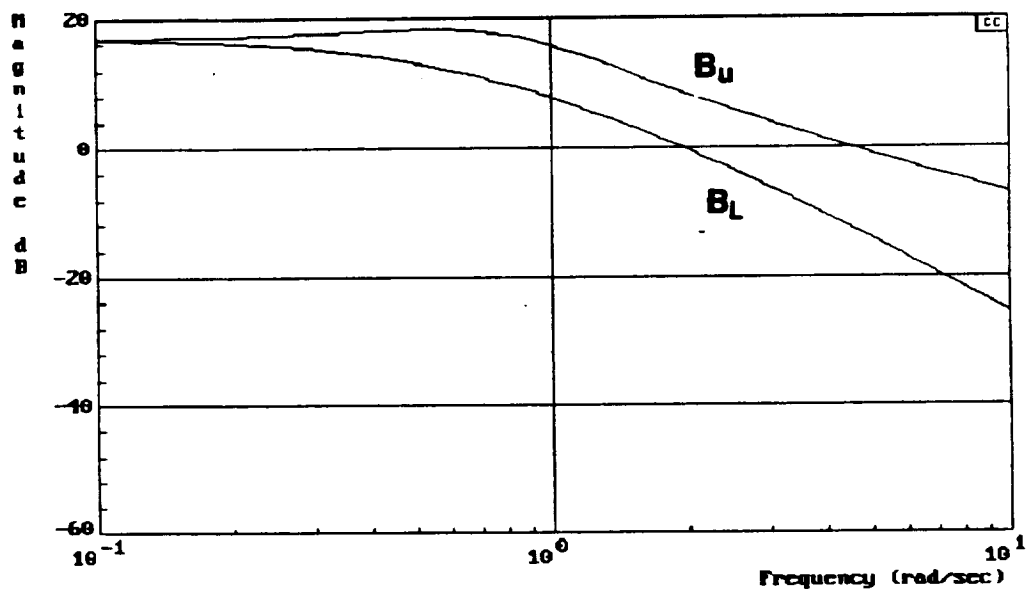


Figure 20. Performance specification in frequency domain for approach and landing of B-720 TOFC

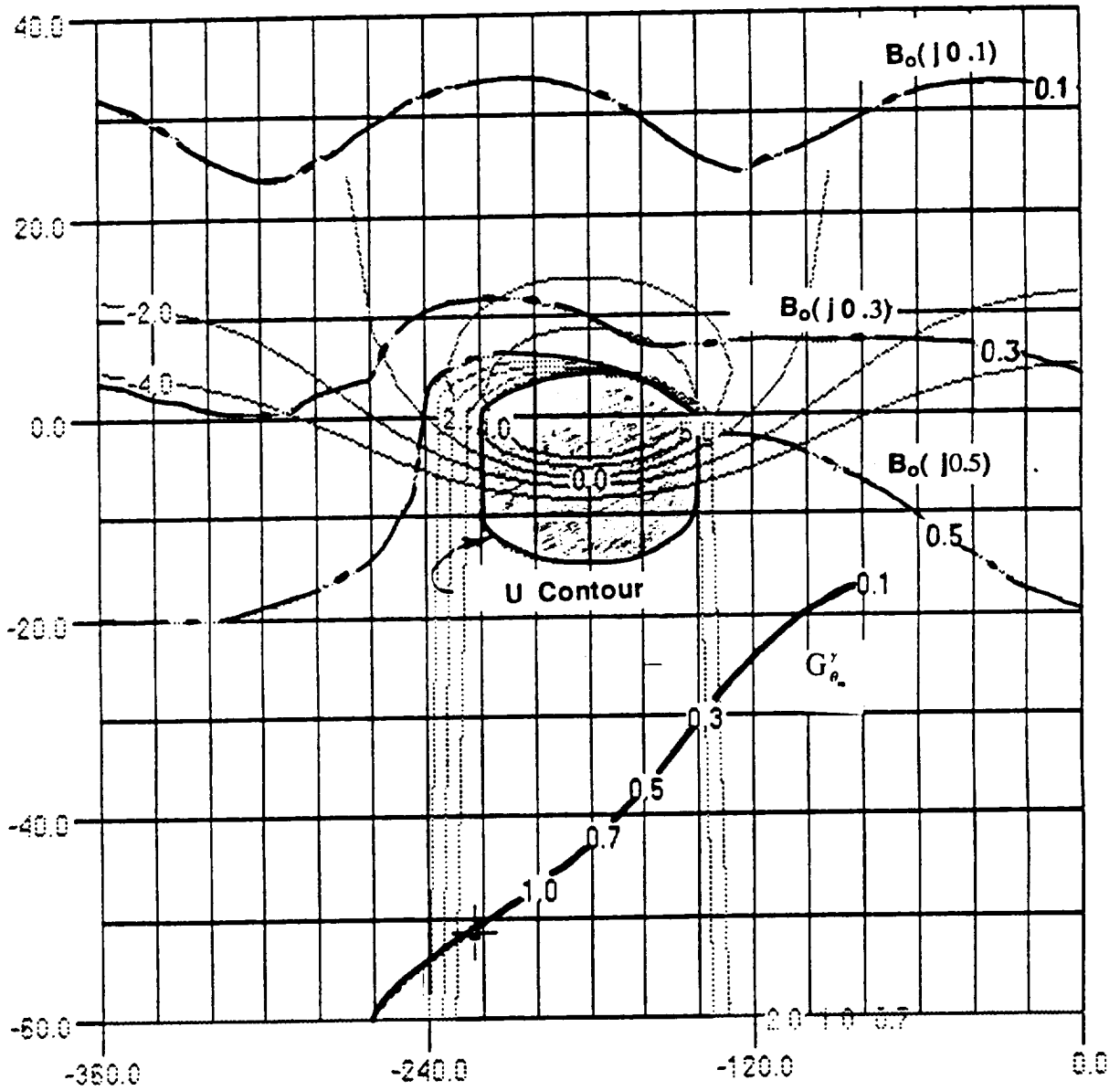


Figure 21. Transfer function  $G'_m$ , its performance bounds  $B(j\omega)$ , and U contour on Nichols Chart

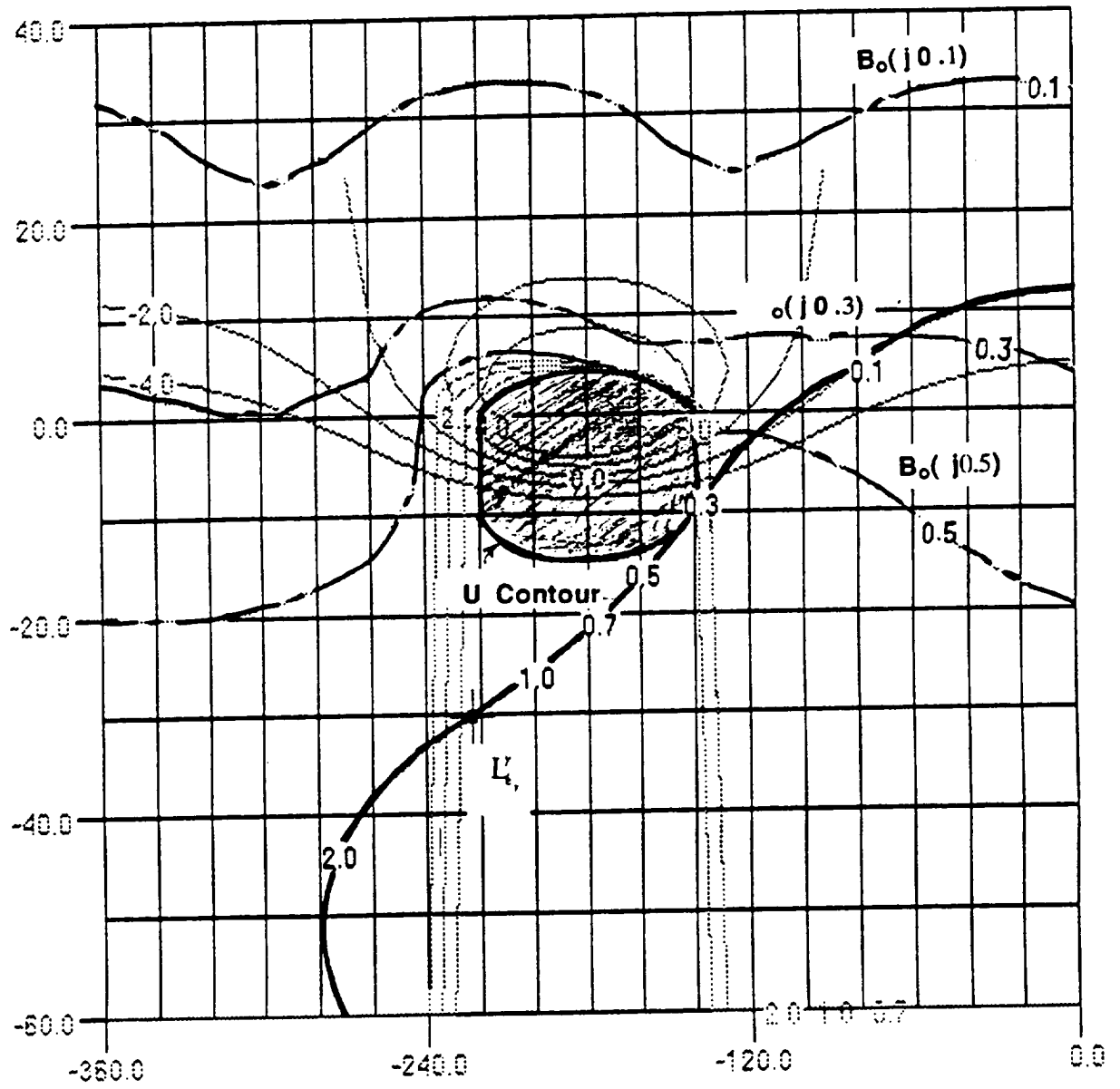


Figure 22. Open-loop transfer function,  $L'_{om}$ , on Nichols Chart

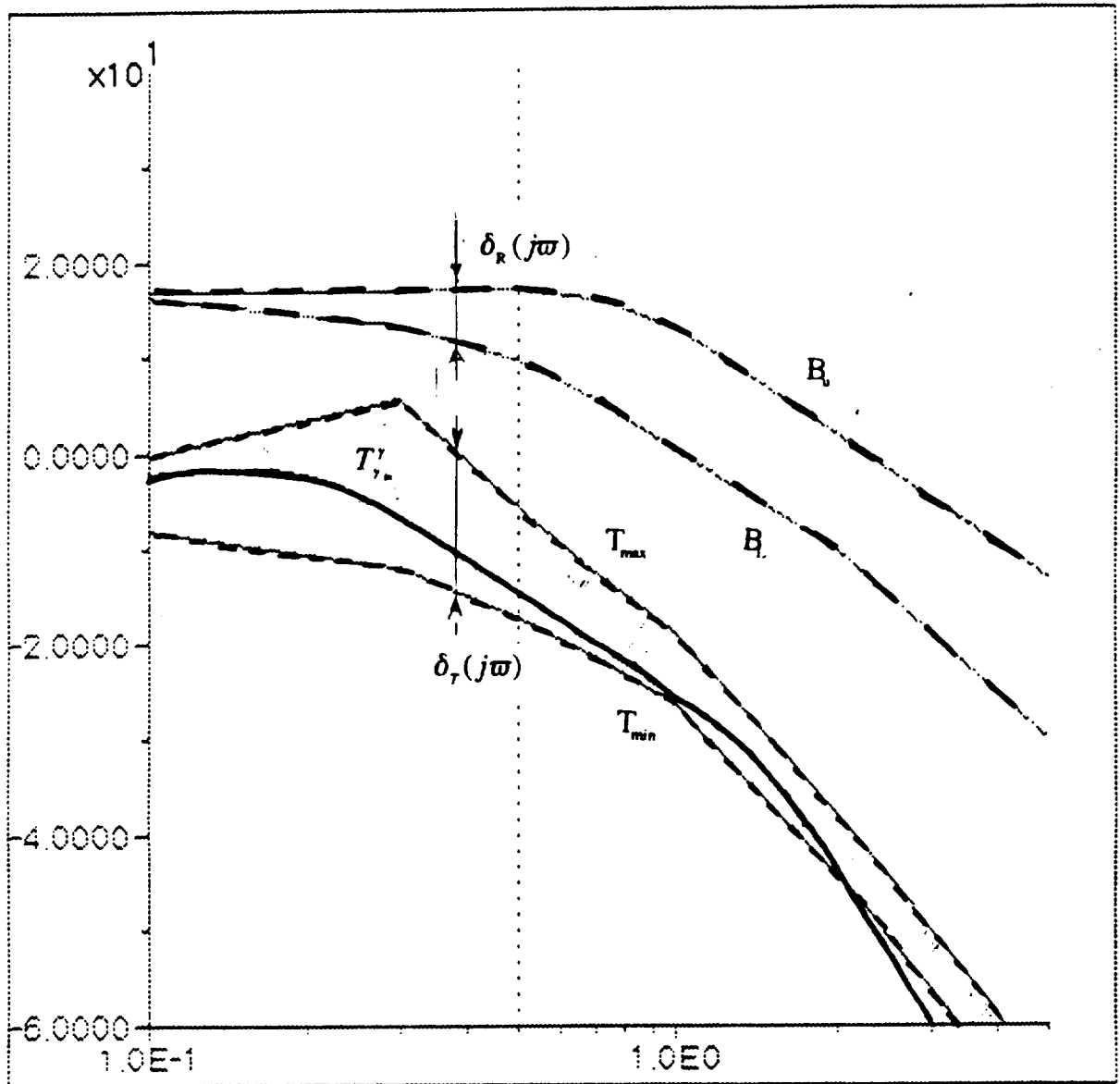


Figure 23. Frequency plot of the close-loop transfer function  $T'_{m}$  with no prefilter

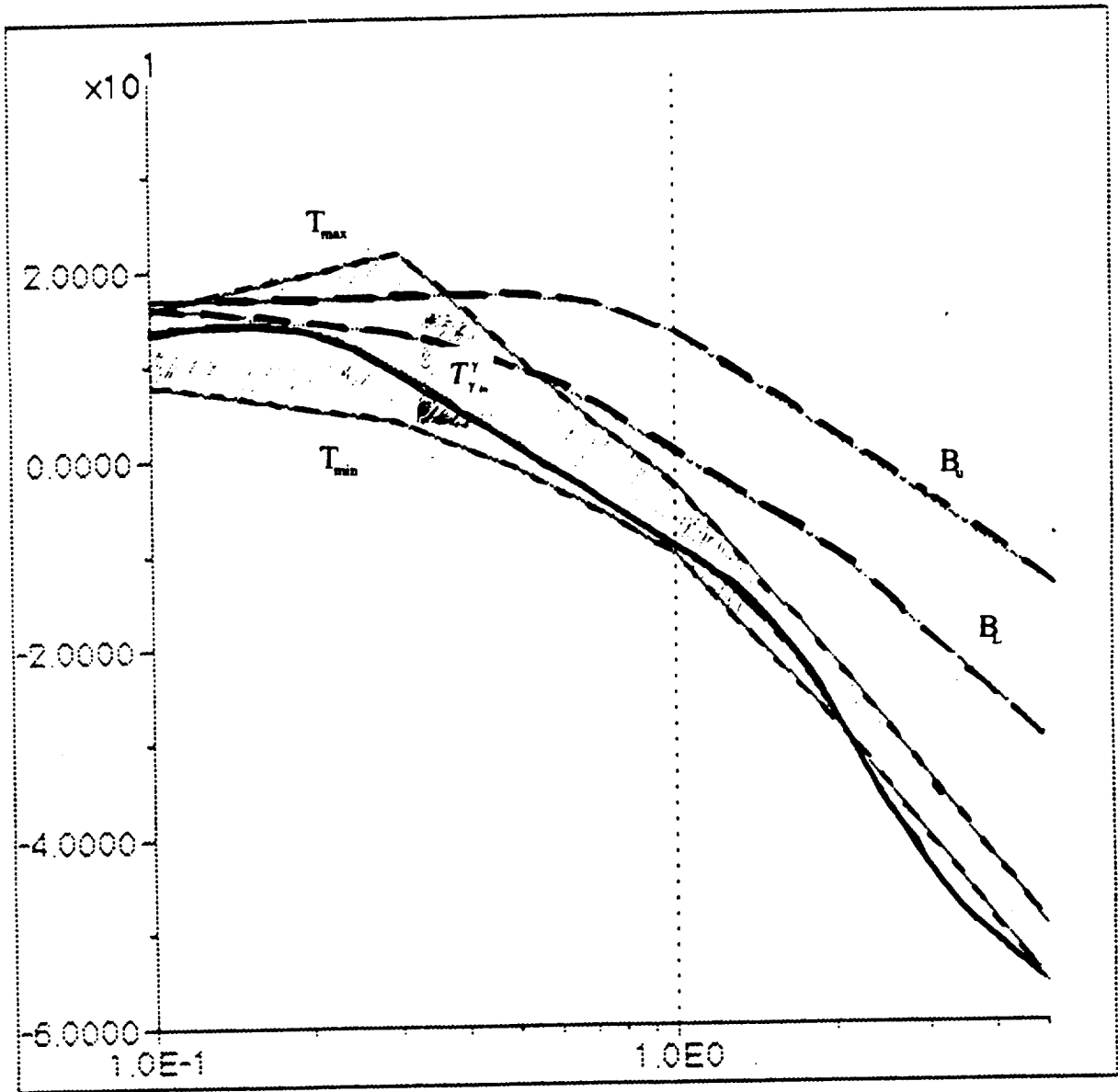


Figure 24. Frequency plot of the close-loop transfer function  $T_{r_m}^c$  with prefilter

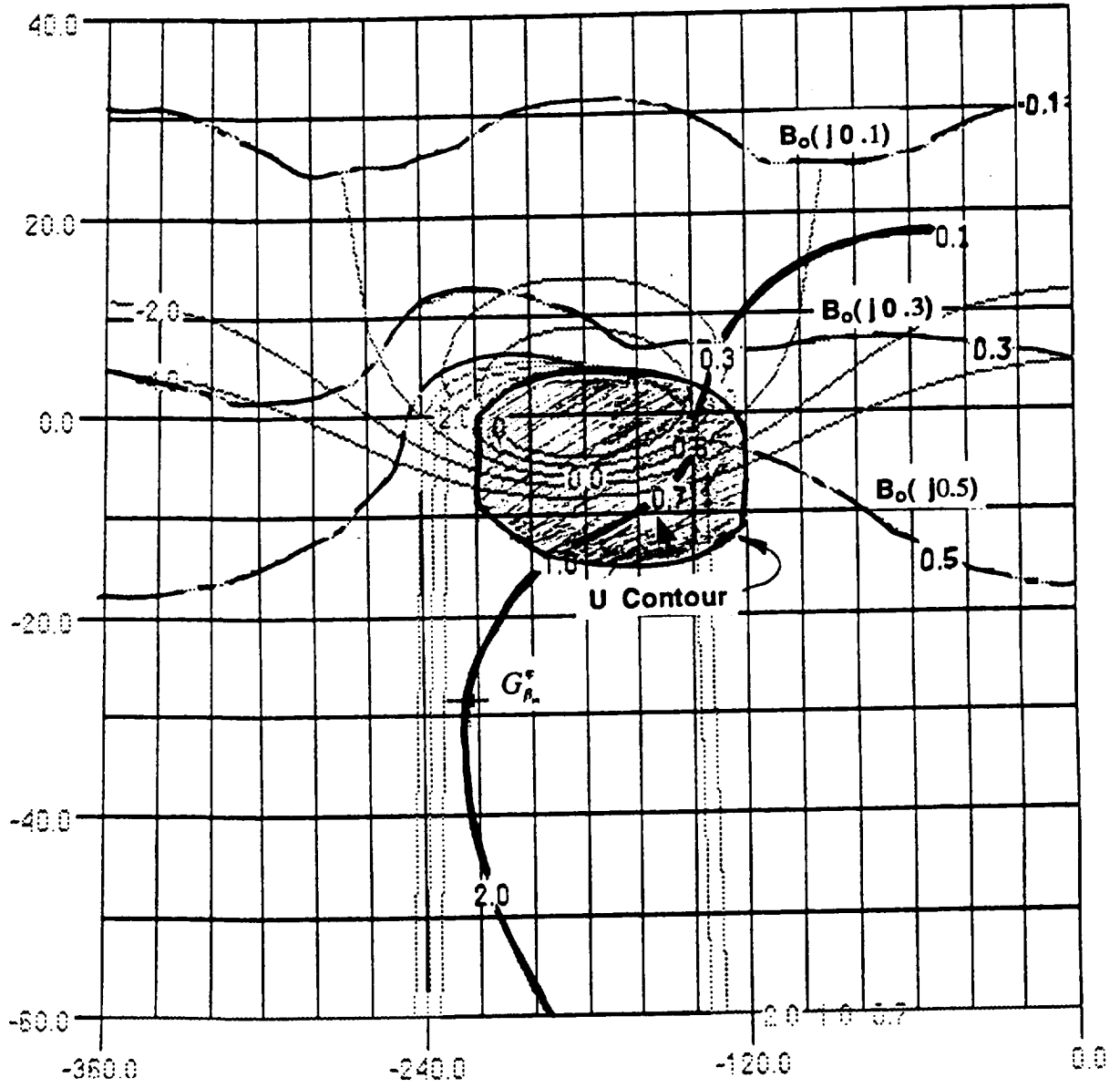


Figure 25. Transfer function  $G_{\rho_m}^*$ , its performance bounds  $B(j\omega)$ , and U contour on Nichols Chart

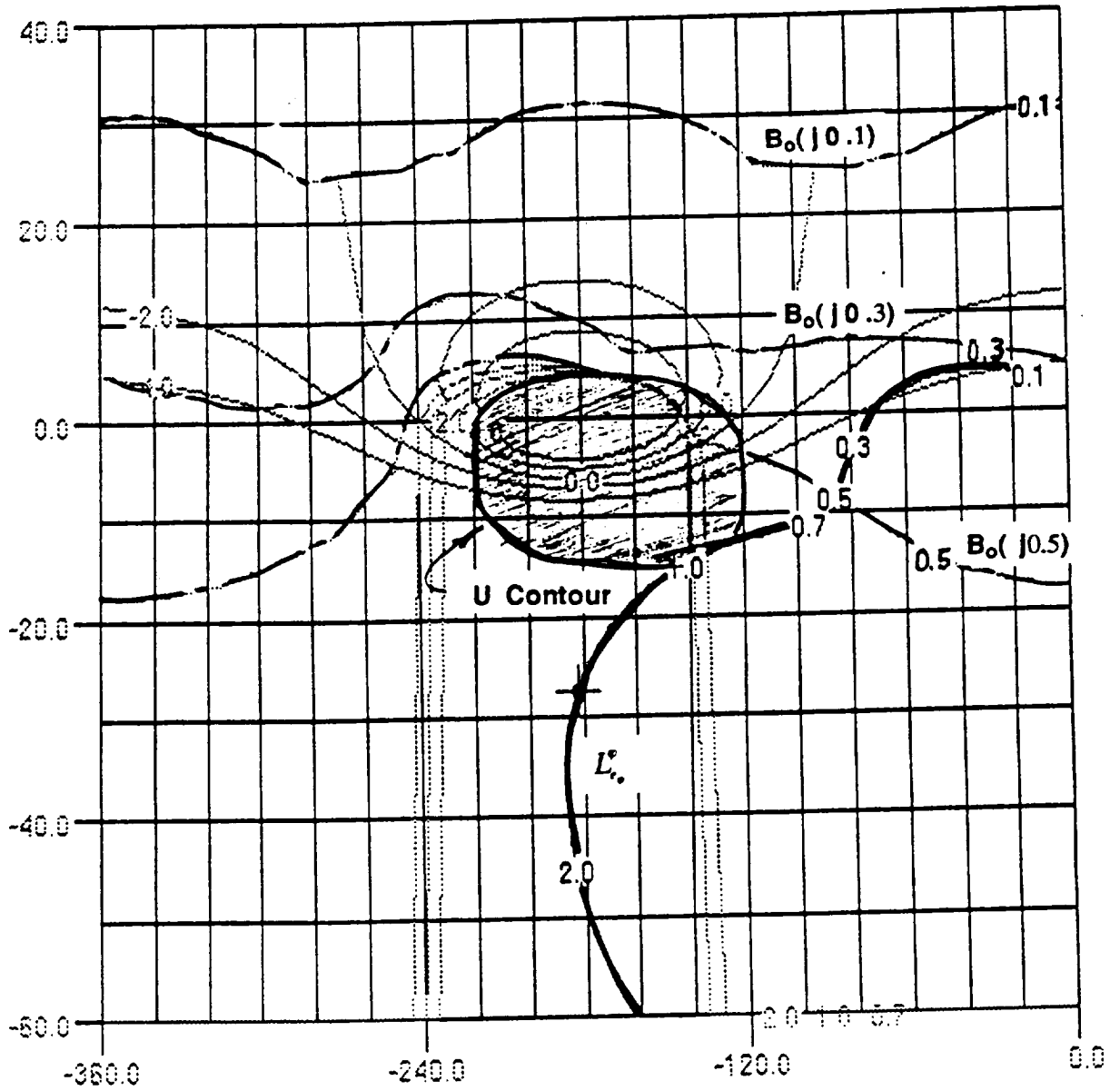


Figure 26. Open-loop transfer function,  $L_o^*$ , on Nichols Chart

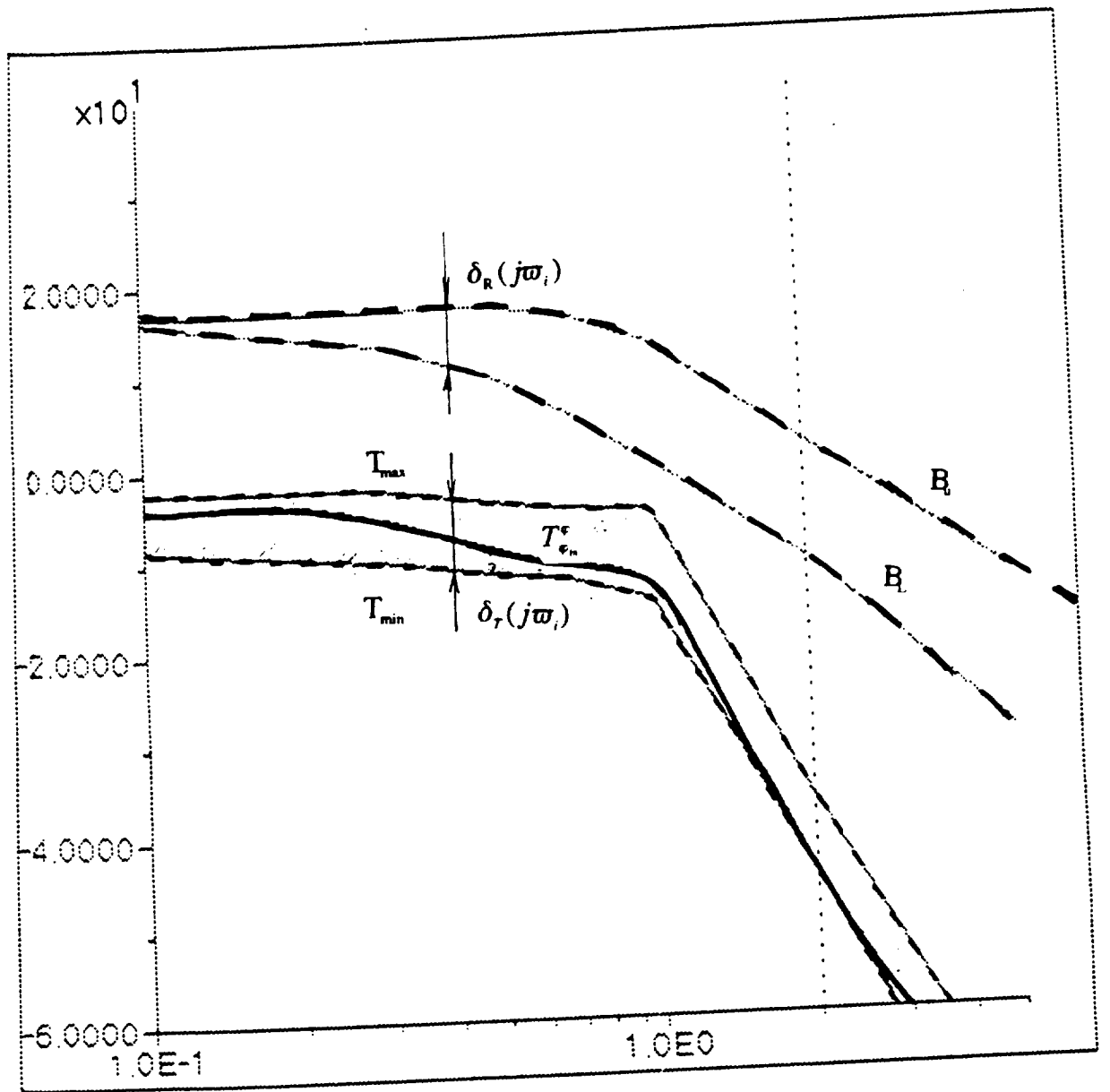


Figure 27. Frequency plot of the close-loop transfer function  $T_{rn}^*$  with no prefilter

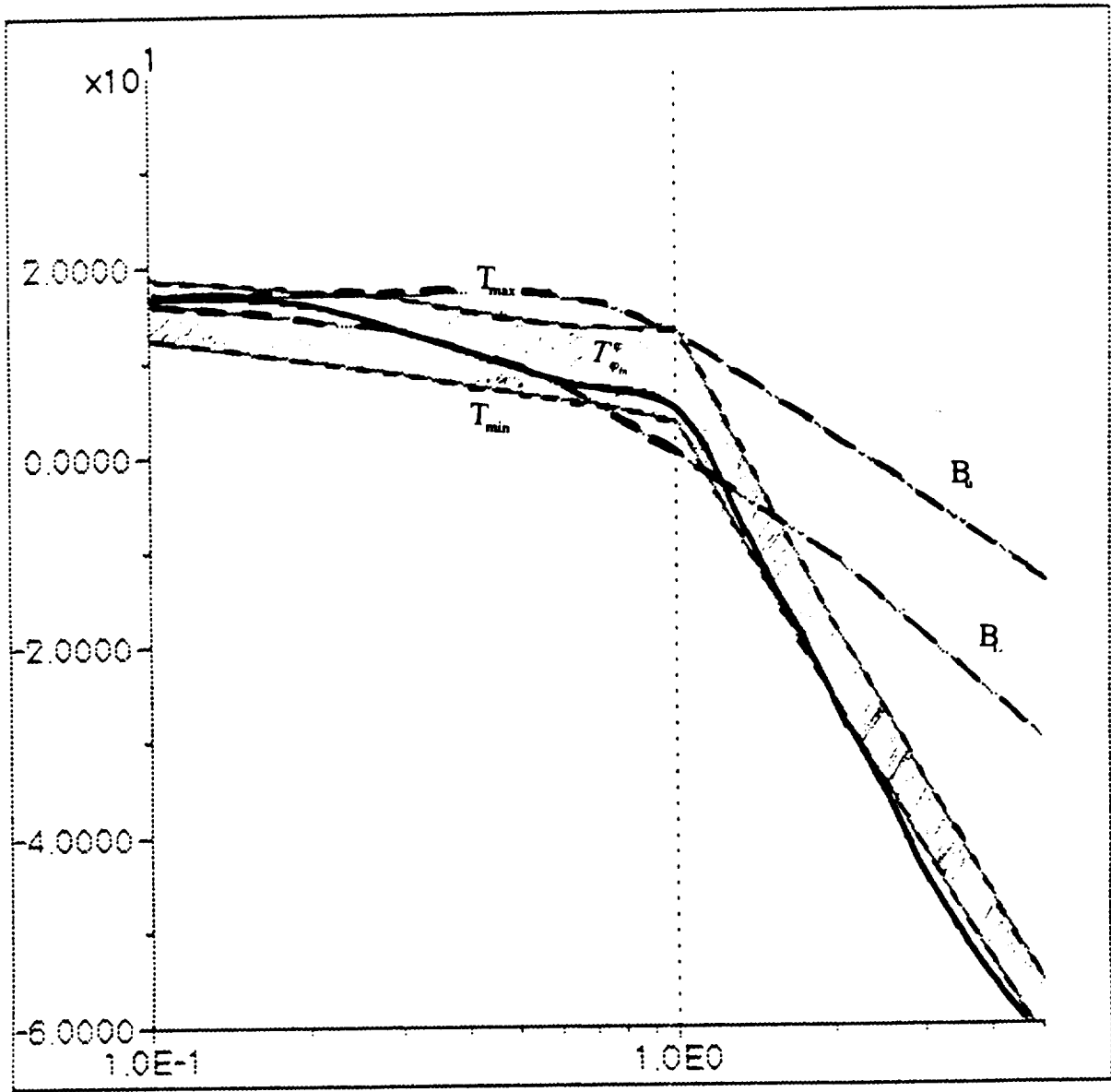


Figure 28. Frequency plot of the close-loop transfer function  $T_{\phi_n}^*$  with prefilter

### Longitudinal Response

2 degree flight path angle cmd

--- : Simulation compensation

— : QFT compensation

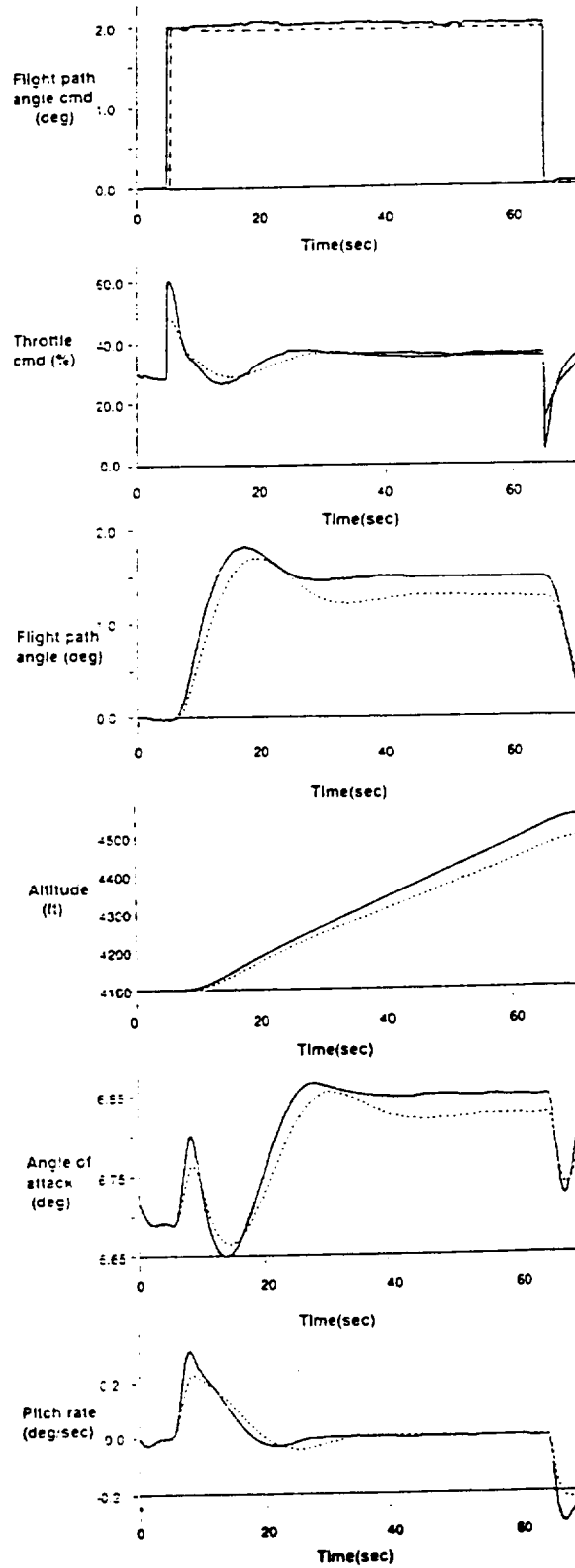


Figure 29. B-720 augmented control, step flight-path-angle response with no turbulence, nominal configuration

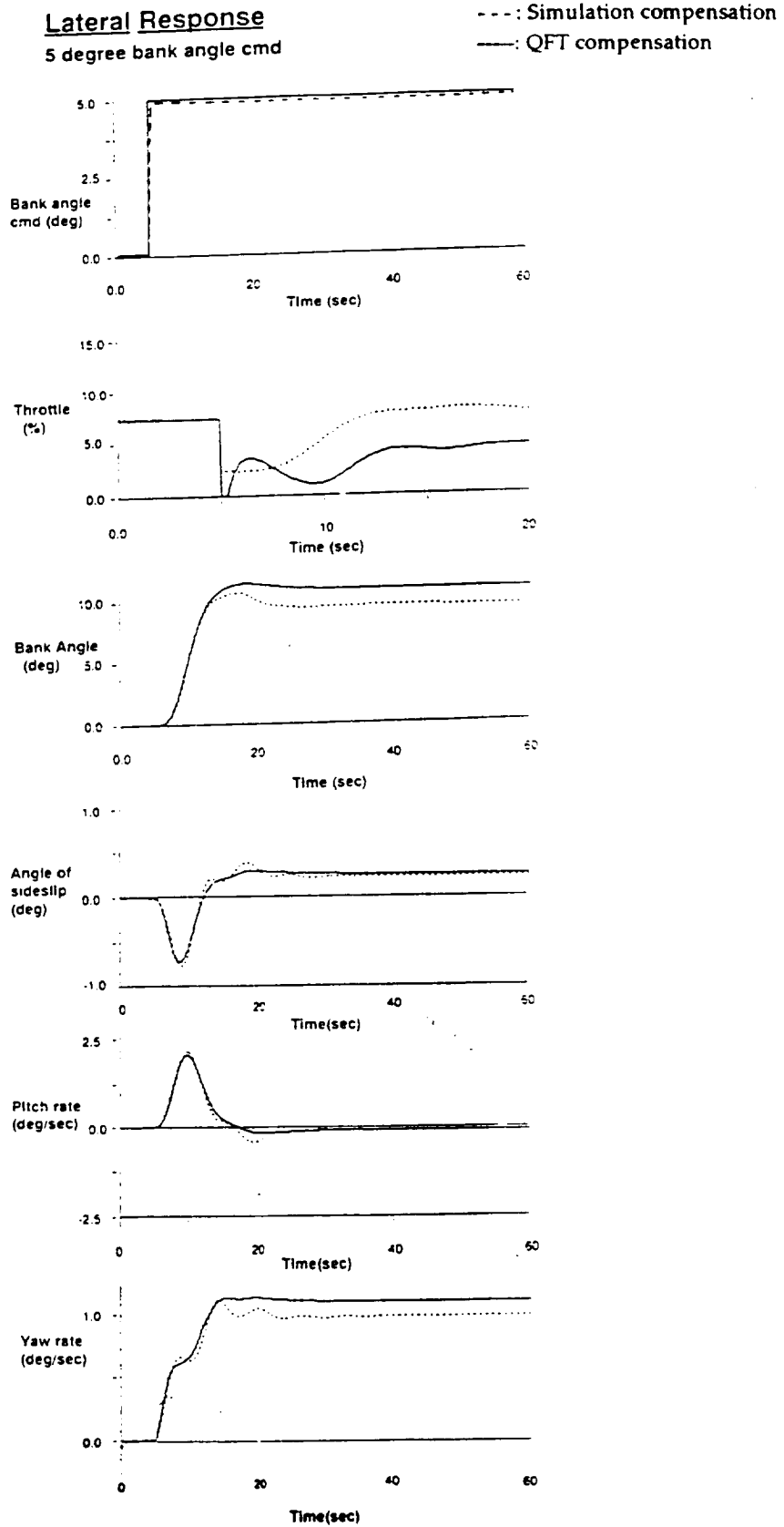
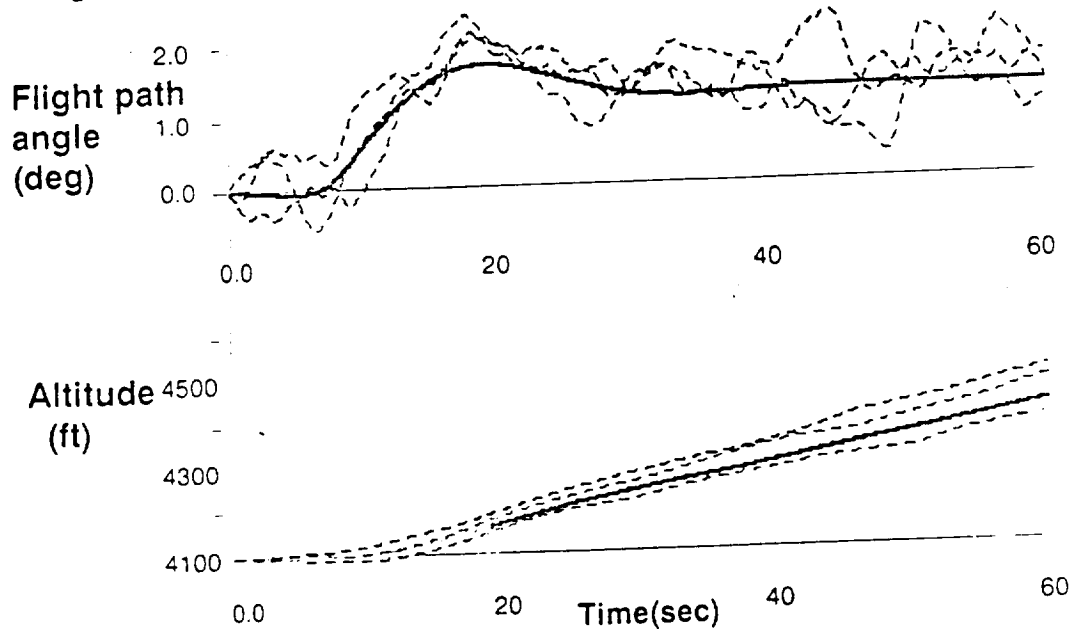


Figure 30. B-720 augmented control, step bank-angle response with no turbulence, nominal configuration

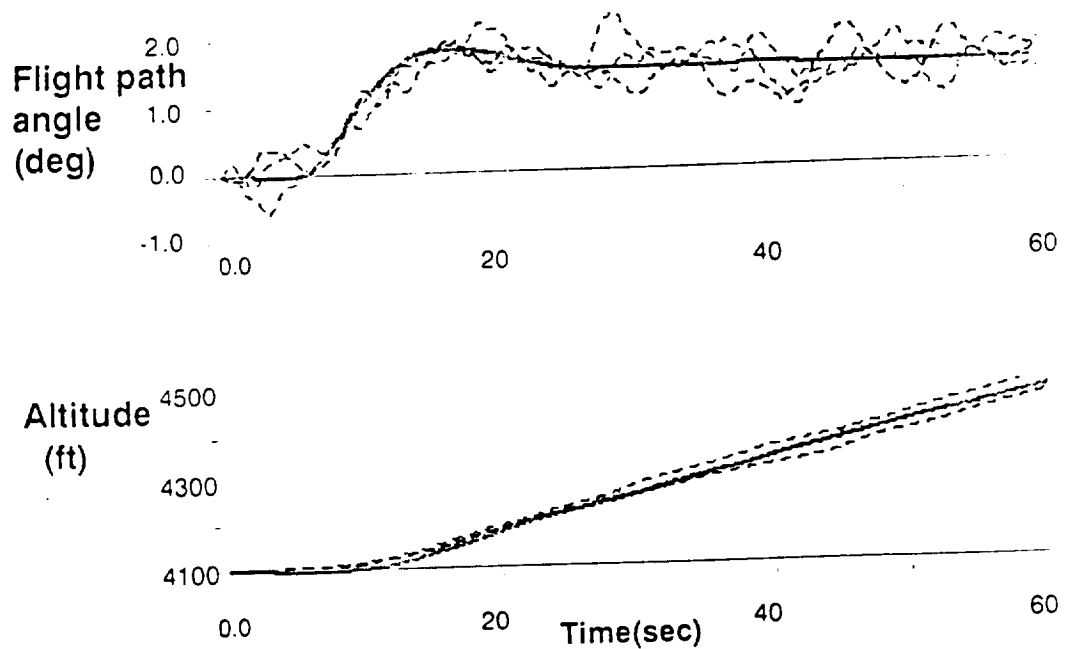
### Longitudinal Response

2 degree flight path angle command

— : no turbulence  
- - - : intermediate turbulence



a) Simulation Compensation

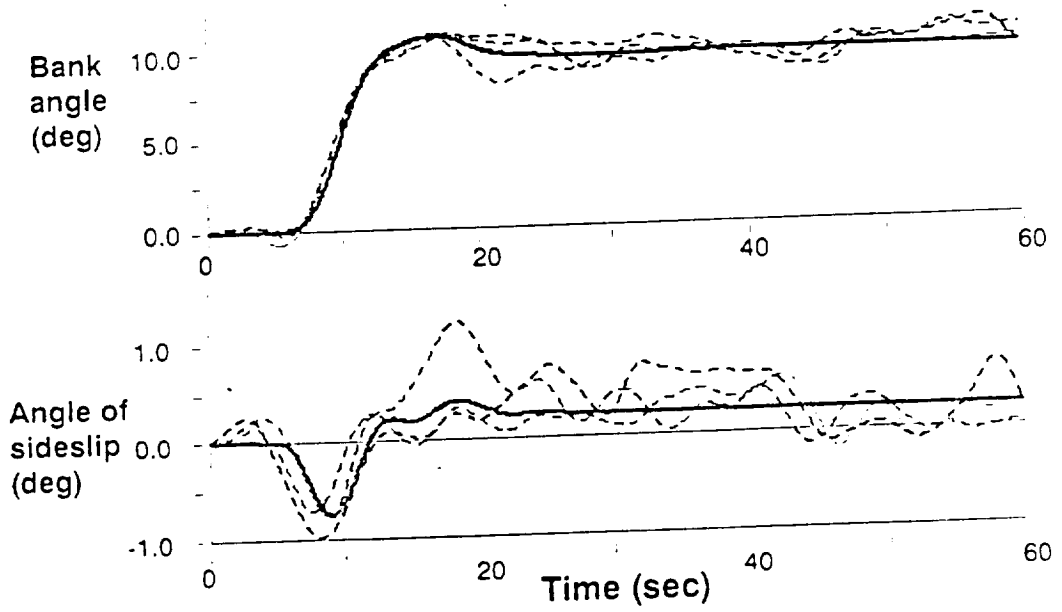


b) QFT Compensation

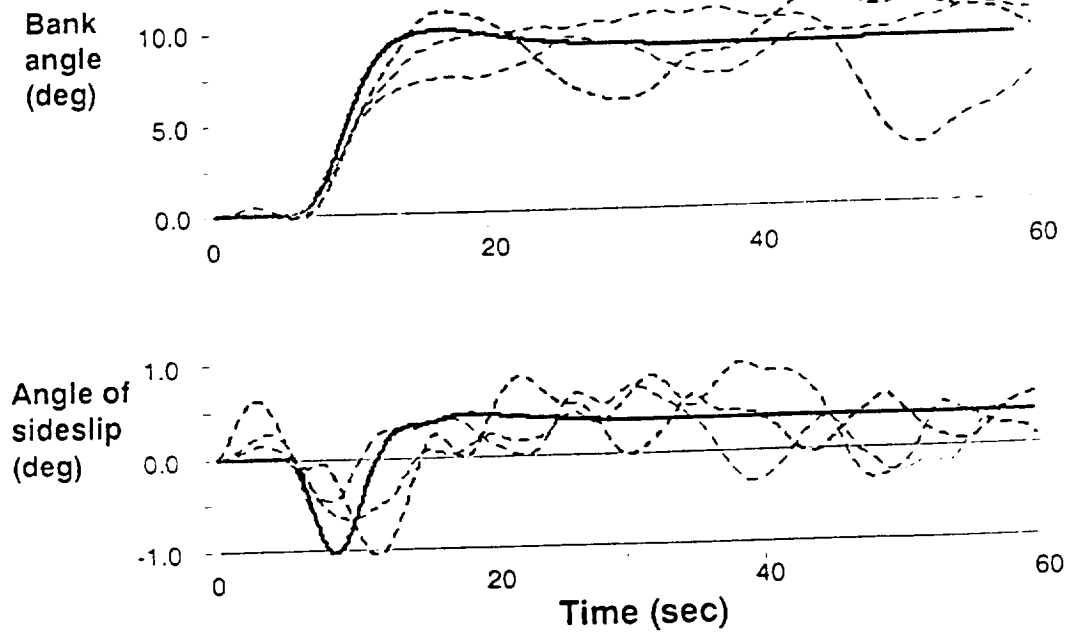
Figure 31. B-720 augmented control, step flight-path-angle response with turbulence, nominal configuration

**Lateral Response**  
5 degree bank angle command

----- : no turbulence  
- - - - : intermediate turbulence



a) Simulation Compensation



b) QFT Compensation

Figure 32. B-720 augmented control, step bank-angle response with turbulence, nominal configuration

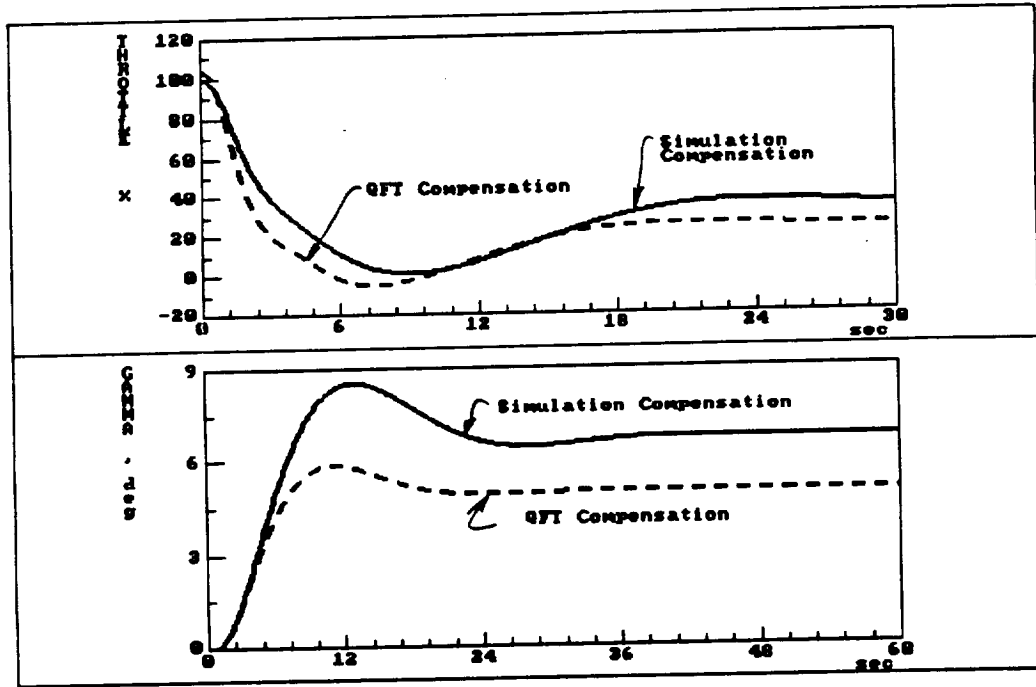


Figure 33. Flight-path-angle and throttle response to full-forward stick deflection, nominal configuration

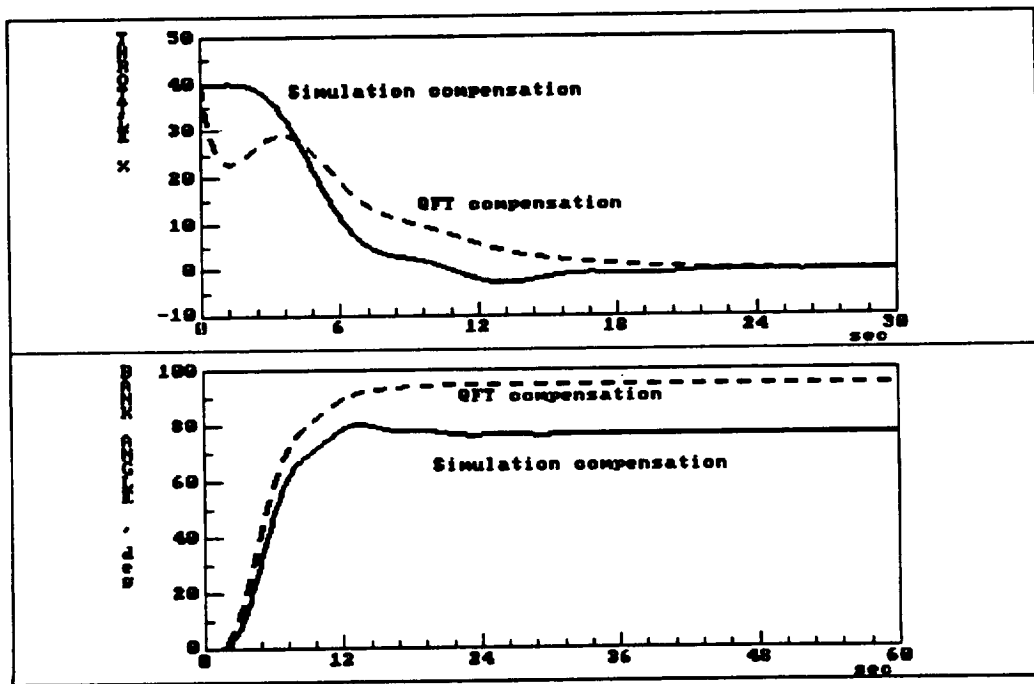


Figure 34. Bank-angle and throttle response to full-right stick deflection - QFT compensation, nominal configuration

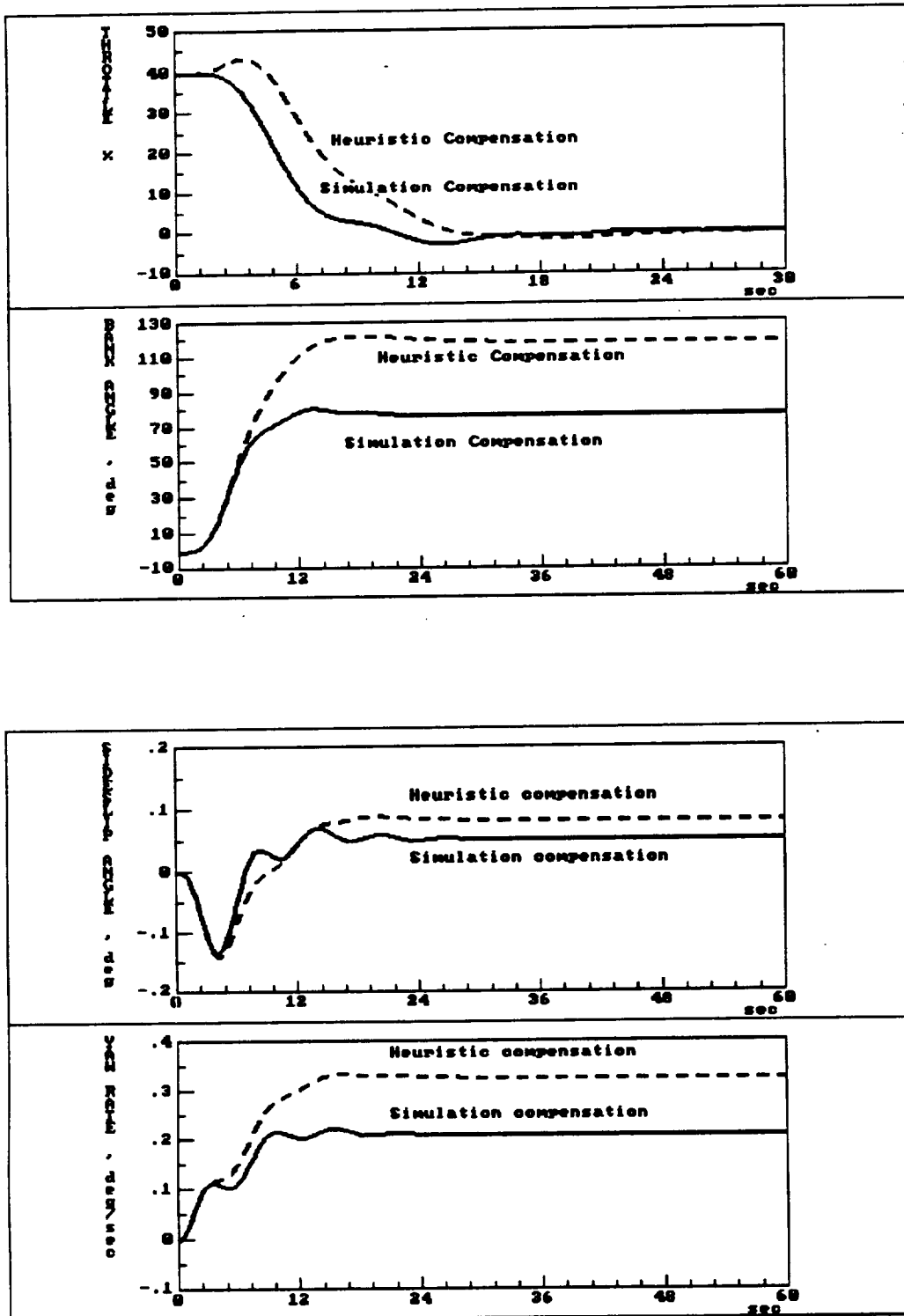


Figure 35. Response to full-right stick deflection - Heuristic compensation, nominal configuration

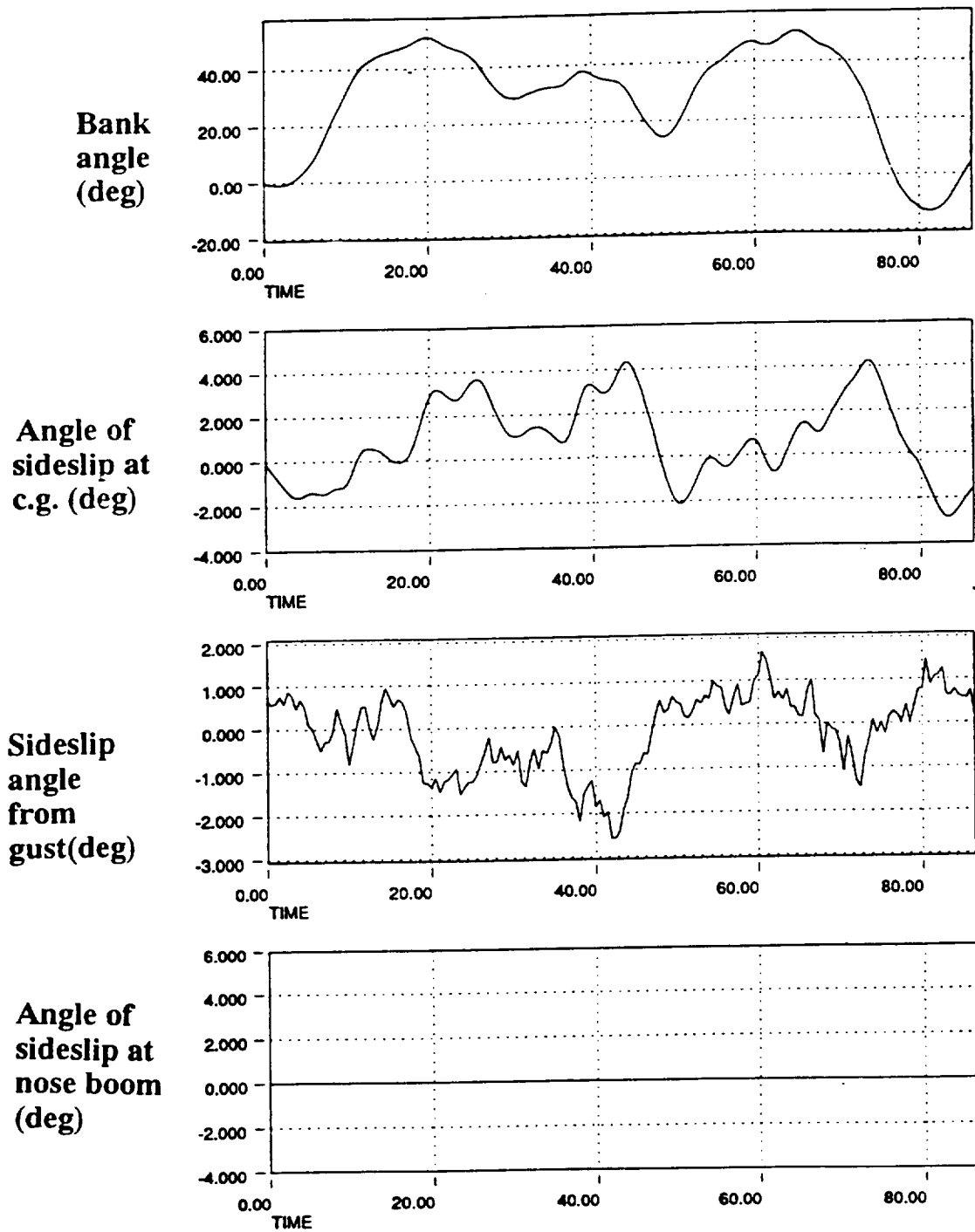


Figure 36. Bank-angle response under turbulence due to c.g.  $\beta$

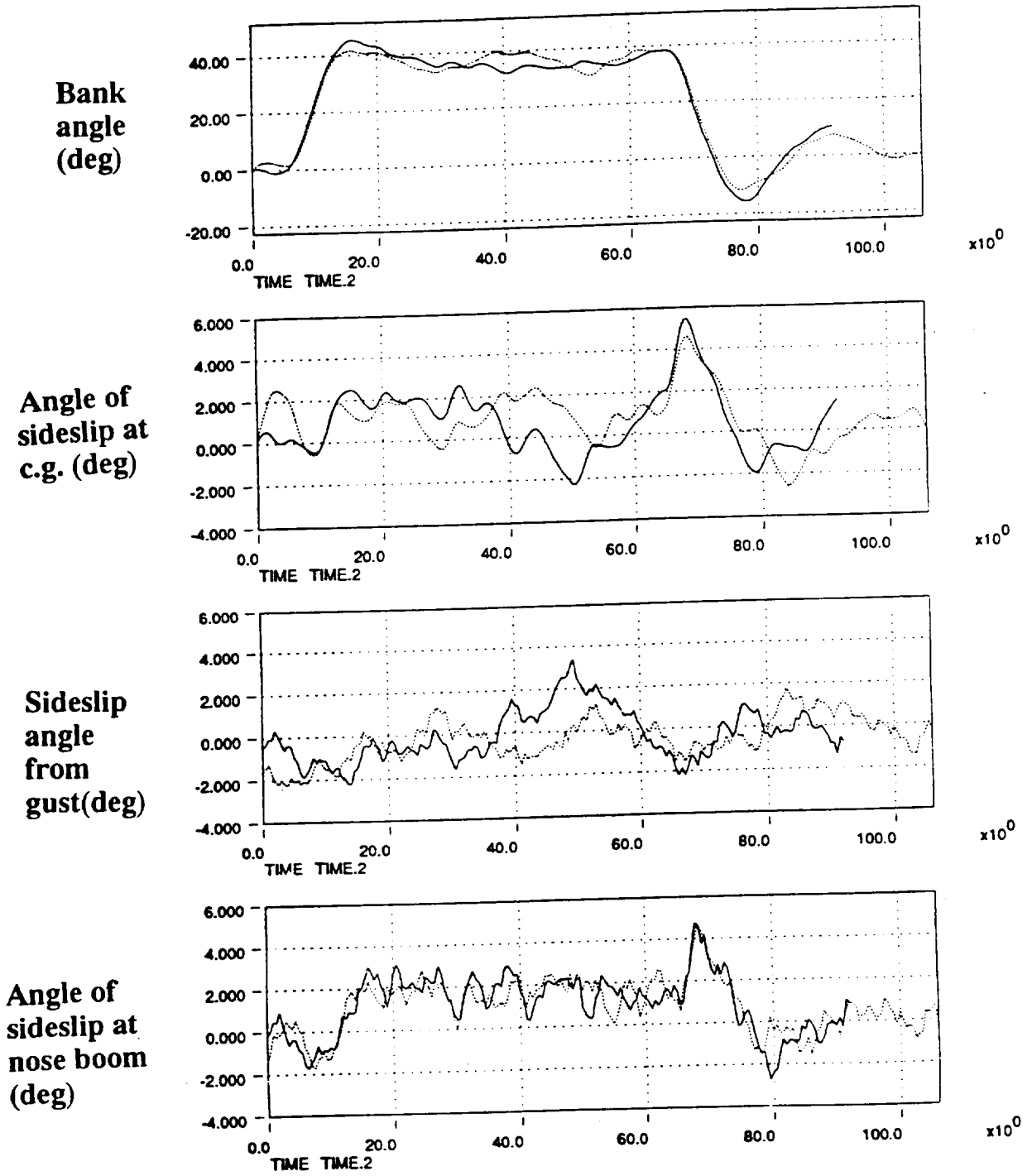
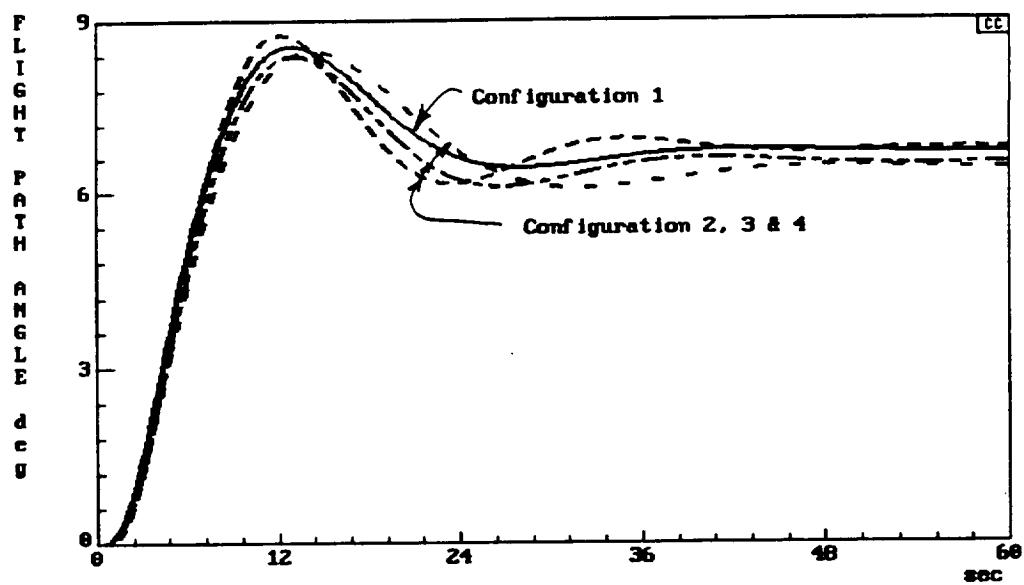
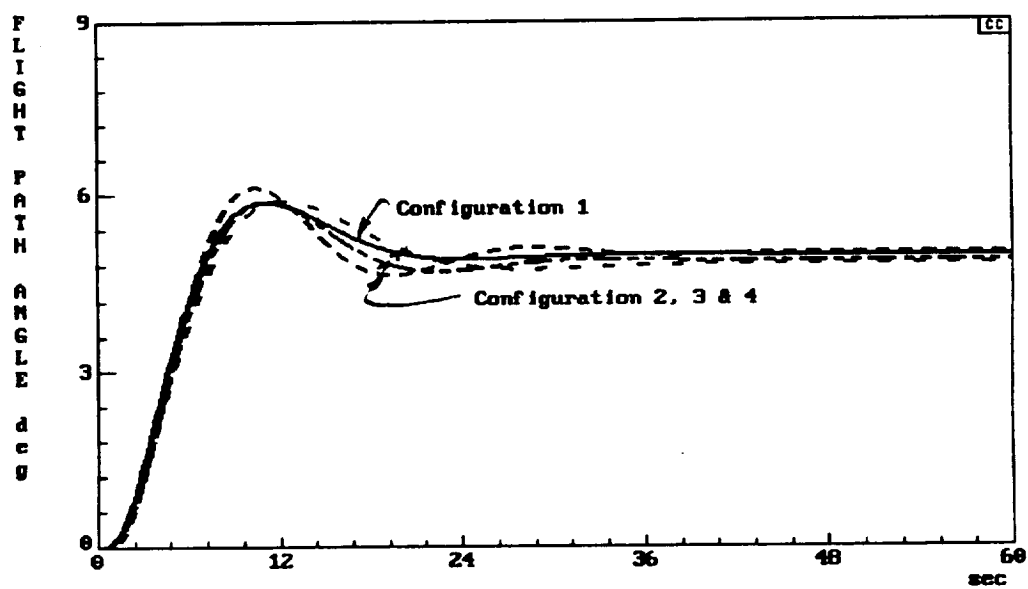


Figure 37. Bank-angle response under turbulence due to nose boom  $\beta$

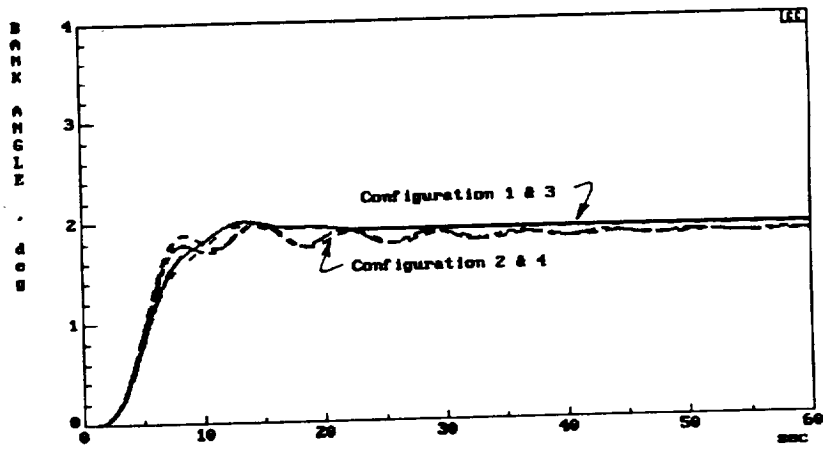


a) Simulation Compensation

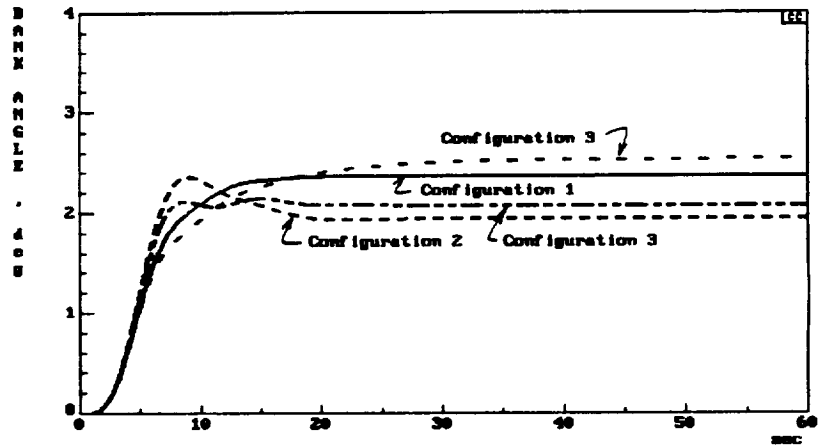


b) QFT Compensation

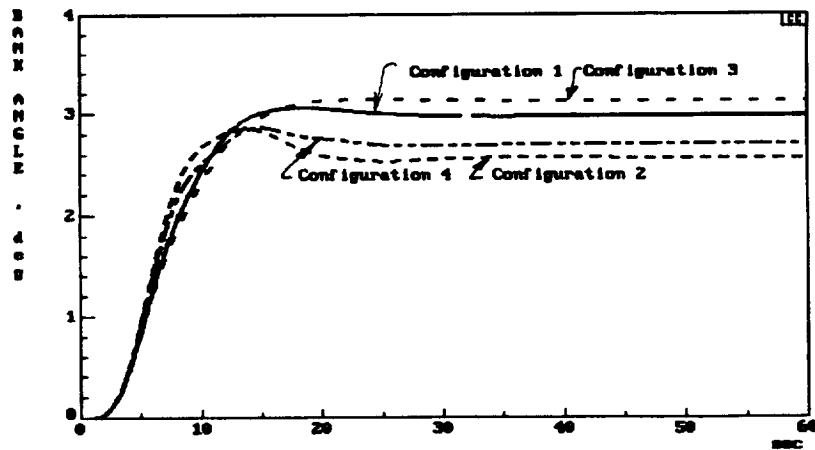
Figure 38. Robustness of the flight-path-angle control



a) Simulation Compensation



b) QFT Compensation

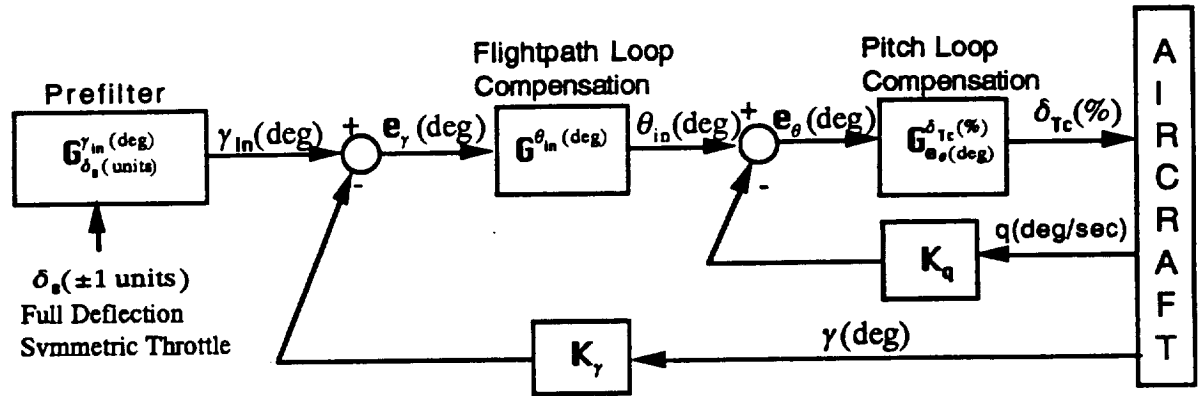


c) Heuristic compensation

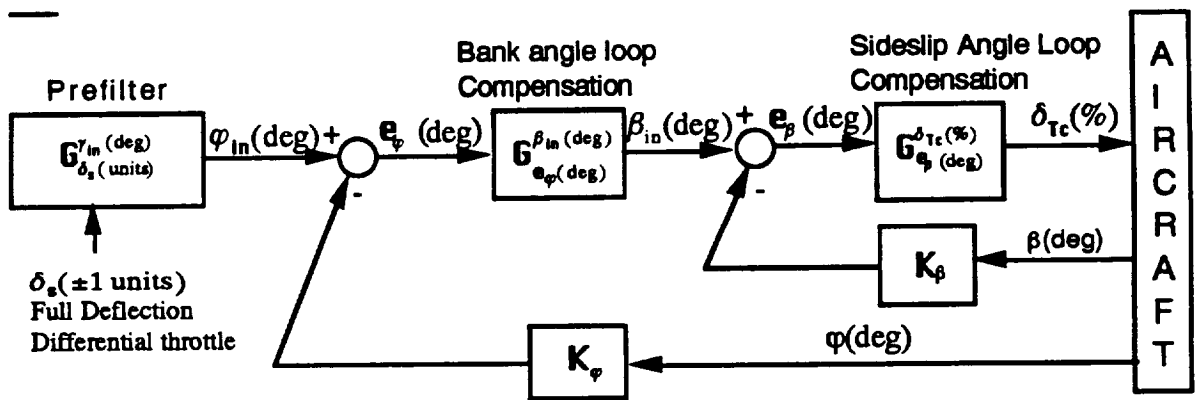
Figure 39. Robustness of the bank-angle control

## APPENDIX A: B-720 CONFIGURATIONS

The B-720 piloted simulation can be represented by the following block diagram:



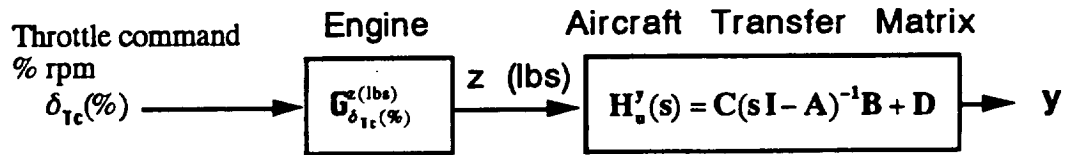
**Flightpath Angle Control Simulation**



**Bank Angle Control Simulation**

The "AIRCRAFT" in the box above represents both the engine and the bare airframe dynamics. The engine is approximated by a transfer function,  $G_{eng}$ , and the bare airframe dynamics are represented mathematically by a single quadruple,  $P_{a/c}$ , shown as follows:

## Longitudinal Dynamics



$$P_{s/c} = \begin{bmatrix} \dot{x} \\ y \end{bmatrix} = \begin{bmatrix} A & B \\ C & D \end{bmatrix} \quad \text{throttle inputs equal} \quad \begin{bmatrix} A & B_1(\text{column}) \\ C & D = 0 \end{bmatrix}$$

$$x = [q(\text{deg/sec}) \mid \alpha(\text{deg}) \mid v(\text{kts}) \mid \theta(\text{deg}) \mid h(\text{ft})]'$$

$$y = [n_{\text{pilot}} \mid n_{\text{cog}} \mid q \mid \alpha \mid v \mid \theta \mid h \mid \gamma(\text{deg})]'$$

$$u = [z_{\text{outbd left}}(\text{lbs}) \mid z_{\text{inbd left}}(\text{lbs}) \mid z_{\text{inbd right}}(\text{lbs}) \mid z_{\text{outbd right}}(\text{lbs})]'$$

$$u_1 = z(\text{lbs}) \quad \text{[used when all throttles have same command]}$$

## Lateral Dynamics

$$\begin{bmatrix} \dot{x} \\ y \end{bmatrix} = \begin{bmatrix} A & B \\ C & D \end{bmatrix} \begin{bmatrix} x \\ u \end{bmatrix} = \begin{bmatrix} A & B_2 \\ C & D = 0 \end{bmatrix} \begin{bmatrix} x \\ u_2 \end{bmatrix}$$

where

$$P_{s/c} = \begin{bmatrix} A & B \\ C & D \end{bmatrix} \quad \text{.....for four engine inputs, } u$$

$$= \begin{bmatrix} A & B_2 \\ C & D = 0 \end{bmatrix} \quad \text{.....for one total engine input, } u_2$$

$$x = [p(\text{deg/sec}) \mid r(\text{deg/sec}) \mid \beta(\text{deg}) \mid \phi(\text{deg})]'$$

$$y = [A_{Y_{c.g.}} \mid p(\text{deg/sec}) \mid r(\text{deg/sec}) \mid \beta(\text{deg}) \mid \phi(\text{deg})]'$$

$$u = [z_{\text{outbd left}}(\text{lbs}) \mid z_{\text{inbd left}}(\text{lbs}) \mid z_{\text{inbd right}}(\text{lbs}) \mid z_{\text{outbd right}}(\text{lbs})]'$$

$$u_2 = [z(\text{lbs})], \quad \text{where } z = z_{\text{outbd left}} + z_{\text{inbd left}} + (-z_{\text{inbd right}}) + (-z_{\text{outbd right}})$$

The B matrix has four columns, each column is to be multiplied by the thrust input from each engine that is given in matrix u. If symmetric throttle is given (assume all four throttles are given the same command), the B matrix in longitudinal dynamics becomes a single column. Each row value in this column matrix  $B_1$  is equal to the sum of the corresponding row elements in

the full order **B** matrix representing four engines. If differential throttle is given (i.e., the left engines and right engines are given same amount of command but in opposite directions), the **B** matrix in lateral dynamics becomes another single column matrix, **B<sub>2</sub>**. Each row element in **B<sub>2</sub>** is the sum of the positive value of columns 1 and 2, and the negative value of columns 3 and 4 of each row in **B**. The open-loop configuration then becomes **P=Pa/c\*Peng**, where **Peng** is the quadruple form of the engine transfer function, **G<sub>h(s)</sub><sup>(\*)</sup>**. The quadruples for four different configurations were obtained as described in reference.

Flight conditions for each configuration are summarized in the following table.

### Configuration Summary

| Config. Number | Weight (lbs) | Altitude (Ft MSL) | Airspeed (Knots) | Flaps (%) | Gear up/down |
|----------------|--------------|-------------------|------------------|-----------|--------------|
| 1              | 140,000      | 4,000             | 160              | 0         | up           |
| 2              | 140,000      | 4,000             | 145              | 30        | up           |
| 3              | 160,000      | 4,000             | 175              | 0         | up           |
| 4              | 140,000      | 4,000             | 155              | 30        | up           |

The transfer functions were obtained from the quadruples using System Technology's Program CC. These aircraft transfer functions are listed here with each respective row of numbers designating the corresponding configuration transfer function values. The nominal configuration, number 1, is represented by values in each row 1 below.

### Longitudinal Transfer Functions

$$N_{z(\text{lbs})}^{q(\text{deg/sec})} = N_{z(\text{lbs})}^{q(\text{deg/sec})} / \Delta_{\text{long}}$$

$$N_{z(\text{lbs})}^{\gamma(\text{deg})} = N_{z(\text{lbs})}^{\gamma(\text{deg})} / \Delta_{\text{long}}$$

$$N_{z(\text{lbs})}^{q(\text{deg/sec})} = \begin{array}{cccc} \hline 2.36\text{E}-04 & (0) & (-1.17\text{E}-05) & (0.40) & (0.61) \\ \hline 2.33\text{E}-04 & (0) & (1.4\text{E}-06) & (0.635, & 0.563) \\ \hline 1.976\text{E}-04 & (0) & (0.292) & (0.644) & \\ \hline 1.955\text{E}-04 & (0) & (2.68\text{E}-06) & (0.819, & 0.508) \\ \hline \end{array}$$

$$N_{z(lbs)}^{\gamma(deg)} = \begin{array}{c} \hline 2.796E-05 \quad (0) \quad (0.203) \quad (0.370, \quad 3.008) \\ \hline -1.819E-05 \quad (0) \quad (0.364) \quad (2.255) \quad (-4.452) \\ \hline 2.130E-05 \quad (0.167) \quad (0.351, \quad 3.038) \\ \hline 1.470E-05 \quad (0) \quad (0.261) \quad (0.460, \quad 3.426) \\ \hline \end{array}$$

$$\Delta_{long} = \begin{array}{c} \hline (1.438E-05) \quad (3.918E-02, \quad 0.130) \quad (0.652, \quad 1.382) \\ \hline (1.101E-05) \quad (7.423E-02, \quad 0.147) \quad (0.596, \quad 1.375) \\ \hline (3.949E-02, \quad 0.118) \quad (0.649, \quad 1.301) \\ \hline (1.878E-05) \quad (7.190E-02, \quad 0.138) \quad (0.588, \quad 1.279) \\ \hline \end{array}$$

### Lateral Transfer Functions

$$N_{z(lbs)}^{\beta(deg)} = N_{z(lbs)}^{\beta(deg)} / \Delta_{lat}, \quad N_{z(lbs)}^{\beta(deg)} = \begin{array}{c} \hline -1.58E-03 \quad (-.0805) \quad (.927) \\ \hline -1.59E-03 \quad (-.0922) \quad (.904) \\ \hline -1.43E-03 \quad (-.0723) \quad (.981) \\ \hline -1.44E-03 \quad (-.0879) \quad (.940) \\ \hline \end{array}$$

$$N_{z(lbs)}^{\phi(deg)} = N_{z(lbs)}^{\phi(deg)} / \Delta_{lat}, \quad N_{z(lbs)}^{\phi(deg)} = \begin{array}{c} \hline 3.19E-04 \quad (.468, \quad 3.65) \\ \hline 2.15E-04 \quad (.611, \quad 4.17) \\ \hline 2.89E-04 \quad (.447, \quad 3.96) \\ \hline 2.04E-04 \quad (.593, \quad 4.33) \\ \hline \end{array}$$

$$\Delta_{lat} = \begin{array}{c} \hline (.0001) \quad (1.01) \quad (.116, \quad 1.05) \\ \hline (.006) \quad (1.05) \quad (.067, \quad 0.93) \\ \hline (.0028) \quad (1.06) \quad (.114, \quad 1.08) \\ \hline (.0065) \quad (1.09) \quad (.060, \quad .944) \\ \hline \end{array}$$

The engine transfer function for all configurations is given in short form notation by:

$$G_{s, \omega}^{z(lbs)} = \frac{275}{(0.55)(s)}$$

Configuration Storage Table for Quadruples

\*Pxxxx.4U : Quadruple with four engine inputs

\*Pxxxx.1U : Quadruple with one total engine input

| Dynamics     | Config. Number | Quadruple Pa/c | Quadruple Pa/c*Peng |
|--------------|----------------|----------------|---------------------|
| Longitudinal | 1              | P1000.4U       | -                   |
|              | 1              | P1000.1U       | P100                |
| Longitudinal | 2              | P2000.4U       | -                   |
|              | 2              | P2000.1U       | P200                |
| Longitudinal | 3              | P3000.4U       | -                   |
|              | 3              | P3000.1U       | P300                |
| Longitudinal | 4              | P4000.4U       | -                   |
|              | 4              | P4000.1U       | P400                |
| Lateral      | 1              | P5000.4U       | -                   |
|              | 1              | P5000.1U       | P500                |
| Lateral      | 2              | P6000.4U       | -                   |
|              | 2              | P6000.1U       | P600                |
| Lateral      | 3              | P7000.4U       | -                   |
|              | 3              | P7000.1U       | P700                |
| Lateral      | 4              | P8000.4U       | -                   |
|              | 4              | P8000.1U       | P800                |

## **APPENDIX B: PAPERS PRODUCED IN SUPPORT OF THIS GRANT**

1. Biezad, D.J. and C.P. Azzano. "Designing Low Bandwidth Propulsive-Only Flight Controllers." AIAA Guidance, Navigation, and Control Conference Paper No. 91-2628CP. New Orleans, LA. August 12-14, 1991. 267-275.
2. Biezad, D.J. "The Propulsive-Only Flight Control Problem." National Aerospace Electronics Conference, Vol. 2. Dayton, OH. May 20-24, 1991. 494-500.
3. Biezad, D.J. and H.L. Chou. "Pilot-in-the-Loop Analysis of Propulsive-Only Flight Control Systems." NAECON, Vol. 2. Dayton, OH. 482-488.
4. Biezad, D.J. and H.L. Chou. "Application of QFT to the Problem of Failed In-Flight Controllers During Approach and Landing of a B-720 Aircraft." To be presented at NAECON 93. Dayton, OH. May 24-28, 1993.